Mitochondrial variation in *Anopheles gambiae* and *An. coluzzii*: phylogeographic legacy of species isolation and mito-nuclear associations with metabolic resistance to pathogens and insecticides

Running title: Mitogenome evolution in the *Anopheles gambiae* complex

Jorge E. Amaya Romero[1,2]†, Clothilde Chenal[2,3], Yacine Ben Chehida[1,4], Alistair Miles[5], Chris S. Clarkson[5], Vincent Pedergnana[2], Bregje Wertheim[1], Michael C. Fontaine[1,2]*†

Affiliations

1. Groningen Institute for Evolutionary Life Sciences (GELIFES), University of Groningen, Nijenborgh 7, 9747 AG Groningen, Netherlands.
2. MIVEGEC, Univ. Montpellier, CNRS, IRD, Montpellier, France.
3. Institut des Science de l'Evolution de Montpellier, Univ Montpellier, CNRS, Montpellier, France
4. Ecology and Evolutionary Biology, School of Biosciences, University of Sheffield, Sheffield, S10 2TN, UK
5. Wellcome Sanger Institute, Hixton, Cambridge CB10 1SA, UK

† contributed equally to the study.

*** Correspondance :** Michael C. Fontaine (michael.fontaine@cnrs.fr). MIVEGEC (U. Montpellier, CNRS, IRD), Centre IRD Occitanie, 911 Avenue Agropolis, BP 64501, 34394 Montpellier Cedex 5, France

ORCID

- YBC : https://orcid.org/0000-0001-7269-9082
- AM : https://orcid.org/0000-0001-9018-4680
- VP : https://orcid.org/0000-0002-7852-5339
- BW : https://orcid.org/0000-0001-8555-1925
- MCF : https://orcid.org/0000-0003-1156-4154

Abstract

Mitochondrial DNA (mtDNA) has been a popular neutral marker in phylogeography, phylogeny, and molecular ecology, but its complex evolution is increasingly recognized. Here, we investigated mtDNA variation in *An. gambiae* and *An. coluzzii*, in perspective with other species in the *Anopheles gambiae* complex (AGC), by assembling the mitogenomes of 1219 mosquitoes across Africa. The mtDNA phylogeny of the AGC was consistent with a previously reported highly reticulated evolutionary history, revealing important discordances with the species tree. The three most widespread species (*An. gambiae, An. coluzzii*, *An. arabiensis*), known for extensive historical introgression, could not be discriminated based on mitogenomes. Furthermore, a monophyletic clustering of the three salt-water tolerant species (*An. merus*, *An. melas*, *An. bwambae*) in the AGC also suggested that introgression and possibly selection shaped mtDNA evolution. MtDNA variation in *An. gambiae* and *An. coluzzii* across Africa revealed significant partitioning among populations and species. A peculiar mtDNA lineage found predominantly in *An. coluzzii* and in the hybrid taxon of the African "*far-west*" exhibited divergence comparable to the inter-species divergence in the AGC, with a geographic distribution matching closely *An. coluzzii*'s geographic range. This phylogeographic relict of the *An. coluzzii* and *An. gambiae* split was associated with population and species structuration, but not with *Wolbachia* occurrence. The lineage was significantly associated with SNPs in the nuclear genome, particularly in genes associated with pathogen and insecticide resistance. These findings underline the mito-nuclear coevolution history and the role played by mitochondria in shaping metabolic responses to pathogens and insecticide in *Anopheles*.

Keywords: *Anopheles gambiae*, mitogenome, mitochondria, mtDNA, mito-nuclear coevolution, speciation genomics, phylogeography, Wolbachia, insecticide resistance, plasmodium, malaria vector, insect

Introduction

Historically, mitochondrial DNA (mtDNA) has been among the most popular genetic markers in molecular ecology, evolution, and systematics. Among its applications are assessing population and species genetic diversity, genetic structure, phylogeographic and phylogenetic patterns, species identity and meta-barcoding (Galtier, et al. 2009; Dong, et al. 2021; Dowling and Wolff 2023). Contributing factors to such popularity include an easy access to the mtDNA genetic variation compared to nuclear markers, even in degraded tissue samples, due to the large number of per-cell copies. Likewise, its haploid nature and clonal inheritance through the female germ line provide an account of evolution independent, and complimentary, to the nuclear DNA's (nuDNA). Because the mtDNA does not recombine, the entire molecule behaves as a single segregating locus, with a single genealogical tree representative of the maternal genealogy. Furthermore, its reduced effective population size together with an elevated mutation rate compared to the nuclear genome makes the mtDNA a fast-evolving, and potentially highly informative genetic marker (Galtier, et al. 2009; Allio, et al. 2017; Dong, et al. 2021; Dowling and Wolff 2023). At the same time, however, the fact that mtDNA is a single non-recombining locus limits its power to describe the evolutionary history of populations and species.

Another argument in favor of mtDNA's popularity as a genetic marker is its near-neutrality and constant mutation rate, but increasing number of studies now contend that selection and other factors can significantly impact mtDNA variation and its evolution (Bazin, et al. 2006; Galtier, et al. 2009; Dong, et al. 2021; Dowling and Wolff 2023). Indeed, mtDNA evolution in arthropods and especially insects, can be significantly impacted by cytoplasmic incompatibilities (CI's) with endosymbionts like the *Wolbachia* bacteria (Hurst and Jiggins 2005; Galtier, et al. 2009; Dong, et al. 2021; Dowling and Wolff 2023). Furthermore, epistatic interactions between mitochondrial and nuclear genome are also suspected to modulate mtDNA genetic variation given the key biological processes happening in the mitochondria and the tight coordination between the two genome compartments (Wolff, et al. 2014; Sloan, et al. 2015; Rand, et al. 2018; Dowling and Wolff 2023; Nguyen, et al. 2023). For example, an increasing number of studies in mosquitoes suggests that mitochondrial respiration and the associated production of reactive oxygen species (ROS) play a significant role in mosquito immune response and metabolic processes involved in pathogens and insecticides resistance (Van Leeuwen, et al. 2008; Ding, et al. 2020). These epistatic interactions are often neglected in ecology and evolution due to the limited number of studies with adequate datasets to test for these effects. The determinants of mtDNA variations in mosquitoes can thus be multifarious (Hurst and Jiggins 2005; Bazin, et al. 2006; Galtier, et al. 2009; Cameron 2014; Wolff, et al.

2014). Therefore, in many cases, mtDNA does not follow a simple neutral genetic evolution and its use in molecular ecology, metabarcoding, and phylogeographic studies requires a clear assessment of the various factors potentially influencing its evolution. However, doing so necessitate investigating mtDNA variation in combination with nuclear genomic data. This is now increasingly possible thanks to democratization of whole genome re-sequencing and large-scale genomic consortium projects.

The genomic resources provided by two consortia – the MalariaGEN *Anopheles gambiae 1000 genome (Ag1000G)* consortium (The Ag1000G Consortium 2017, 2020) and the *Anopheles* 16 genomes project (Neafsey, et al. 2013; Fontaine, et al. 2015; Neafsey, et al. 2015) – offer a unique opportunity to explore the determinants of mtDNA variation in two sister mosquito species within the *Anopheles gambiae* species complex (AGC): *Anopheles gambiae* and *Anopheles coluzzii*. The AGC is a medically important group of at least 9 closely related and morphologically indistinguishable mosquito sibling species (White, et al. 2011; Coetzee, et al. 2013; Barrón, et al. 2019; Loughlin 2020; Tennessen, et al. 2021). Three members of this African mosquito species complex (*An. gambiae*, *An. coluzzii*, and *An. arabiensis*) are among the most significant malaria vectors in the world, responsible for the majority of the 619,000 malaria-related deaths in 2021, 96% of which occurred in sub-Saharan Africa and impacted primarily children under the age of five (World Health Organization 2022). The ecological plasticity of these three species contributes greatly to their status as major human malaria vectors (Coluzzi, et al. 2002). In contrast to the other AGC species (*An. quadriannulatus, An. merus, An. melas, An. bwambae, An. amharicus, An. fontenllei*) with more confined geographic distributions, these three species have wide overlapping distributions across diverse biomes of tropical Africa. This ecological plasticity in the AGC is attributed to a large adaptive potential, stemming mainly from three major genomic properties: (1) a strikingly high number of paracentric chromosomal inversion polymorphisms segregating in their genome, which are implicated in adaptation to seasonal and spatial environmental heterogeneities related both to climatic variables and anthropogenic alterations of the landscape, in phenotypic variation such as adaptation to desiccation, or even resistance to pathogens like *Plasmodium sp.* or insecticides (e.g., Coluzzi, et al. 2002; Costantini, et al. 2009; Simard, et al. 2009; Cheng, et al. 2012; Ayala, et al. 2017; Riehle, et al. 2017; Cheng, et al. 2018); (2) an exceptional level of genetic diversity identified in natural populations provides a rich material onto which natural selection can act (The Ag1000G Consortium 2017, 2020); and (3) a high propensity for hybridization and interspecific gene flow connecting directly or indirectly the gene pools from all the species over the evolutionary time-scale of the complex (Crawford, et al. 2015; Fontaine, et al. 2015; Thawornwattana, et al. 2018; Müller, et al. 2021).

120

121 The species of the AGC radiated within the past 400 to 500 kyrs (Thawornwattana, et al. 2018; Müller, et
122 al. 2021), and the species barriers are not yet fully formed. Although all members of the AGC can be crossed
123 in the laboratory and produce fertile female hybrids but sterile male hybrids (except for *An. gambiae* and
124 *An. coluzzii*), interspecific hybrization rate in nature is supposed to be extremely low (<0.02%) (Pombi, et
125 al. 2017). An exception is the two-sister species *An. gambiae* and *An. coluzzii* which diverged more recently
126 (*ca.* 60 kyr. before present) according to the most recent estimates (Thawornwattana, et al. 2018; Müller,
127 et al. 2021). These two sister species are at an earlier stage of speciation with no post-zygotic isolation
128 detected (reviewed in Pombi, et al. 2017). Hybrid offspring of both sexes are viable and fertile in the
129 laboratory, but strong pre-zygotic and pre-mating isolation barriers have been identified in nature.
130 Hybridization rate is low (*ca.* 1%) across their overlapping distribution range in West Africa, even if high
131 hybridization rates (up to 40%) were reported in the populations from the African "*far west*" (*i.e.* the coastal
132 fringe of Guinea Bissau and Senegambia (estuary of the river Gambia and Casamance in Senegal) (Lee, et
133 al. 2013; Nwakanma, et al. 2013; Pombi, et al. 2017; Vicente, et al. 2017). New unpublished evidence
134 suggests however that these hybrid populations from the African "*far-west"* could be a distinct cryptic
135 hybrid taxon in which diagnostic alleles typically used to discriminate between *An. gambiae* and *An. coluzzii*
136 are still segregating (A. Miles, *pers. comm.*). Nevertheless, despite the low occurrence of contemporary
137 hybridization rates between the members of the AGC, the large geographic overlap in species distributions,
138 together with porous reproductive barriers have resulted in extensive levels for interspecies hybridization
139 over the evolutionary time scales (Fontaine, et al. 2015).

140

141 Extensive introgression rates between species of the AGC combined with elevated levels of incomplete
142 lineage sorting (ILS) due to large effective population sizes contributed to maintain high levels of shared
143 polymorphisms and highly discordant phylogenies along the nuclear genome, greatly hampering the
144 identification of the species evolutionary history (Crawford, et al. 2015; Fontaine, et al. 2015;
145 Thawornwattana, et al. 2018; Müller, et al. 2021). Genome-scale studies depicted a highly reticulated
146 evolutionary history of the AGC with outstanding levels of geneflow being detected between the two-sister
147 species – *An. gambiae* and *An. coluzzii,* and also between *An. arabiensis* and the ancestor of *An. gambiae*
148 and *An. coluzzii*. Most of the genomic regions resistant to introgression on their nuclear genome, and thus
149 informative on the species branching order, were mostly identified in portions of the X chromosome and
150 scattered across less than ~2% of the autosomes (Crawford, et al. 2015; Fontaine, et al. 2015;
151 Thawornwattana, et al. 2018). The lack of any obvious phylogenetic patterns of species structuration at the

152 mitochondrial genome further supported the extensive level of introgression between these three species
153 (Caccone, et al. 1996; Besansky, et al. 1997; Fontaine, et al. 2015; Hanemaaijer, et al. 2018). Additional
154 interspecific introgression signals were also detected between *An. merus* and *An. quadriannulatus*,
155 between *An. gambiae* and *An. bwambae*, and also along the ancestral branches of the AGC species
156 (Thelwell, et al. 2000; Crawford, et al. 2015; Fontaine, et al. 2015; Thawornwattana, et al. 2018; Müller, et
157 al. 2021). Although the selective and evolutionary effects associated with this extensive level of
158 introgression between species of the AGC remains to be fully investigated, clear evidence of adaptive
159 introgression were detected involving chromosomal inversions (Fontaine, et al. 2015; Riehle, et al. 2017;
160 Thawornwattana, et al. 2018) and insecticide resistance loci (Clarkson, et al. 2014; Grau-Bové, et al. 2020;
161 Grau-Bové, et al. 2021; Lucas, et al. 2023).
162
163 Here we leveraged the genomic resources from The Ag1000G Consortium (2017, 2020) and from the
164 *Anopheles* 16 genomes project (Neafsey, et al. 2013; Fontaine, et al. 2015; Neafsey, et al. 2015) to explore
165 the determinants of mitochondrial genetic variation in the *An. gambiae complex* (AGC) with a particular
166 focus on *An. gambiae* and *An. coluzzii*. For that purpose, we first assembled mitogenomes for 1219 pan-
167 African mosquitoes (Fig. 1 and S1) using a new flexible bioinformatic pipeline, called *AutoMitoG* [*automatic*
168 *mitogenome assembly*] (Fig. S2), which relies on *MitoBIM* approach that combines mapping and *de-novo*
169 assembly of short-read sequencing data (Hahn, et al. 2013). We then assessed the level of mtDNA variation,
170 its phylogeographic and population structure, and the mtDNA genealogical history in comparison with the
171 population demographic history previously estimated from the nuclear genome (The Ag1000G Consortium
172 2017, 2020). We further assessed what factors best explain the mtDNA phylogeographic structure, testing
173 various covariates including *Wolbachia* infection status, population structure estimated from nuclear
174 genome data, and chromosomal inversions. Finally, we investigated the mito-nuclear associations that
175 possibly imply coevolution and coadaptation between the two genomic compartments.
176

177 Results and discussion

178 The *AutoMitoG* pipeline and assembly of the Ag1000G mitogenomes

179 The *AutoMitoG* pipeline, which streamlines mitogenome assembly using the MitoBIM approach (see the
180 method section and Fig. S2), successfully assembled 1219 mitogenome sequences from the unmapped
181 short read data originating from the two *An. gambiae* consortia projects (Fontaine, et al. 2015; The
182 Ag1000G Consortium 2017, 2020) (Fig. 1 and S1, Table S1 and S2). We first assessed the pipeline

183 performance by comparing newly assembled mitogenome sequences with those from the 74 samples of
184 the AGC previously generated in Fontaine, et al. (2015) (Fig. S1, Table S1). Average assembly length before
185 any trimming and sequence alignment was 15,366 base pairs (bp). Following Fontaine, et al. (2015) and
186 after sequence alignment, we removed the control region (CR) resulting in a 14,843 bp alignment length.
187 Excluding the CR removed most of the ambiguities and gaps remaining in the alignment (Fig. S3). The
188 previous and present bioinformatic pipelines generated very similar mtDNA assemblies for each sample
189 with one exception (samples ID: Aara_SRS408148, Fig. S4). Beside that sample which resulted from a label
190 mistake in the DRYAD repository of Fontaine, et al. (2015), mitogenome sequence pairs for each sample
191 were nearly identical with a number of nucleotide differences of 0.4 on average (25% quartile: 0.0; 75%
192 quartile: 1.0, max: 3.0) (Fig. S4). We augmented this alignment with newly assembled mitogenome
193 sequences from three *An. bwambae* samples of lower sequencing quality than the other samples (Table
194 S1). These mitogenomes assembled with the two pipelines also generated similar sequences with a slightly
195 lower sequence identity (>99.9%) for each pair of assemblies, except one sample (bwambae_4) which was
196 more difficult to assemble (Fig. S4a and Table S1). Overall, the *AutoMitoG* pipeline performed at a good
197 bench mark level.
198
199 We then applied the *AutoMitoG* pipeline to the 1142 *An. gambiae* and *An. coluzzii* mosquito samples of
200 The Ag1000G Consortium (2020)) (Fig.1, Table S2). Assembly lengths were 15,364 ± 1.9 bp on average (min:
201 15,358 – max: 15,374) (Table S2). The raw alignment was 15,866 bp long, and 14,844 bps after removing
202 the CR and gaps. The 1142 mtDNA sequence alignment of *An. gambiae* and *An. coluzzii* included 3017
203 polymorphic sites (S), 1195 singleton sites (*Sing.*), and a nucleotide diversity (π) of 0.004, defining 910
204 distinct haplotypes (H), with a haplotype diversity (HD) of 0.999 (Table 1).
205

206 **Phylogenetic relationships among mtDNA haplotypes trace the phylogeographic history of the**
207 **species split and introgression among species of the *An. gambiae* complex.**

208 Phylogenetic relationships among the 1142 mtDNA sequences from *An. gambiae* and *An. coluzzii*,
209 together with the 77 mtDNA sequences from the five other species from the AGC (Figure 2, see also Fig. S4
210 and S5) were consistent with previous studies. Indeed, previously reported evidence of extensive gene flow
211 between *An. gambiae*, *An. coluzzii*, and *An. arabiensis* found support in our phylogenetic analyses with a
212 complete absence of any mtDNA haplotype private to *An. arabiensis* samples (Figure 2, see also Fig. S4 and
213 S5). From the mtDNA standpoint, the 12 samples of *An. arabiensis* could not be discriminated from *An.*
214 *gambiae* and *An. coluzzii* as previously reported (Besansky, et al. 1997; Donnelly, et al. 2001; Fontaine, et

215 al. 2015; Hanemaaijer, et al. 2018). Aside from *An. gambiae*, *An. coluzzii*, and *An. arabiensis*, the four other
216 species of the AGC clustered in a monophyletic divergent clade. Within that clade, the three salt-water
217 tolerant species (*An. melas*, *An. merus*, and *An. bwambae*) formed a monophyletic group next to *An.*
218 *quadriannulatus*. One *An. bwambae* sample (bwambae3, Fig. 2 and S4) carried a mtDNA haplotype
219 clustering among those from *An. gambiae*, *An. coluzzii* and *An. arabiensis.* This is consistent with previous
220 evidence of mitochondrial introgression between *An. bwambae* and one of these three species, most likely
221 *An. gambiae* (Thelwell, et al. 2000). Noteworthy, one *An. gambiae* specimen from Cameroon
222 (AN0293_C_CMS, Fig. 2A) carried a unique mitogenome haplotype closely related to *An. quadriannulatus*.
223 This peculiar haplotype likely reflects the historical/original *An. arabiensis* mitogenomes before being fully
224 replaced by those of *An. gambiae* and/or *An. coluzzii* and still segregating at low frequency in the gene pool
225 of the three species. This finding of a "relict" haplotype from the non-recombining mtDNA locus is
226 consistent with the admitted species branching order of the *An. gambiae* species complex, as depicted by
227 the X chromosome (Fontaine, et al. 2015; Thawornwattana, et al. 2018; Müller, et al. 2021). The phase-3
228 of The Ag1000G Consortium (2021), which includes hundreds of samples from *An. arabiensis*, will provide
229 further insights on this topic.

230 While most of the mtDNA haplotypes carried by *An. gambiae*, *An. coluzzii*, and *An. arabiensis* were
231 closely related, as shown by the short branches on the phylogenetic tree (Fig. 2A, Fig. S4 and S5) and on the
232 distance-based non-metric multidimensional scaling (nMDS) (Fig. 2B, Fig. S6), a group of 244 samples (232
233 from the The Ag1000G Consortium (2020) and 12 from Fontaine, et al. (2015)) clustered into a distinctive
234 clade (hereafter called the "cryptic lineage") (Fig. 2A and 2B). This cryptic lineage displayed a higher level
235 of divergence than the others within the mtDNA gene pool of *An. gambiae, An. coluzzii*, *An. arabiensis*, yet
236 similar-to-slightly-lower than for the clades containing the other 4 species of the AGC (Fig. 2A). Interestingly,
237 the geographic distribution of this cryptic group matched closely with the geographic distribution of *An.*
238 *coluzzii*, mostly prevalent in the African "*far-west*" side of the distribution of the two species, and
239 decreasing in frequency eastwards and southwards (Fig. 2C). The prevalence of the cryptic lineage was the
240 most important in the hybrids (taxonomically uncertain) populations where it reached *ca.* 50% of the
241 samples (up to 65% for the populations of the Gambia (GMS) and 40% of the Guinea-Bissau (GWA)), then
242 composing 31% of the *An. coluzzii* samples, and less than 10% of the *An. gambiae* samples (Table 1, Fig. 2C,
243 Fig. S6). This clear enrichment of the cryptic mtDNA lineage in the populations from the African *far-west*,
244 especially in the hybrid and *An. coluzzii* populations, its level of divergence compared to the common
245 mtDNA lineage which was comparable to the levels observed among species of the AGC (Fig. 2), together
246 with the West to East gradient decline, all these observations suggest it could be a phylogeographic legacy

247 of the split between the two sister species, followed by a secondary contact with an incomplete
248 homogenization of the mtDNA gene pool.
249

250 ## Significant mtDNA genetic structure among and within *An. gambiae* and *An. coluzzii*

251 An Analysis of Molecular Variance (AMOVA) (Excoffier, et al. 1992) showed that most of the mtDNA
252 variation was distributed within populations (87.0%), but significant variance partitioning was also
253 observed between populations (9.6%, p<0.001), and between species as well (3.4%, p<0.007) (Table 2).
254 Level of population differentiation (Fig. S7), expressed as F_{ST} values among populations between nuclear
255 genome (nuDNA) from The Ag1000G Consortium (2020) and mtDNA genome were strongly correlated
256 (Fig. S8). F_{ST} values at the nuclear genome explained *ca.* 80% of the mtDNA F_{ST} values ($p < 0.001$). All
257 comparisons involving the isolated island population of Mayotte (FRS) displayed both high values at the
258 nuDNA and mtDNA genome, the highest mtDNA values being observed between the island populations of
259 Mayotte (FRS) and Bioko (GQS) (Fig. S7 and S8). Such elevated levels of mtDNA and nuDNA differentiation
260 reflect the small long-term effective population size and limited gene flow, with potential repeated
261 bottleneck/founder effects. All these contribute to a strong genetic drift of this Mayotte Island
262 populations (FRS), as previously reported (The Ag1000G Consortium 2020). Globally, genetic
263 differentiation observed at the mtDNA were overall higher than those at the nuclear genome, which likely
264 reflect the reduced effective size of the mtDNA compared to the nuDNA. Exceptions included all
265 comparisons involving the taxonomically uncertain and very peculiar population of Kenya (KEA), where
266 the F_{ST} values were lower or equivalent (Fig. S7 and S8). Overall, we observed a high concordance
267 between the mtDNA and nuDNA levels of population differentiation. These results further underline that
268 both geographical location and, to a lesser extent, species differentiations within and between *An.*
269 *gambiae* and *An. coluzzii* are major determinants of mtDNA variation.
270

271 ## MtDNA isolation-by-distance patterns reflect distinct life histories between *An. gambiae* and *An.*
272 *coluzzii*

273 Previous studies showed that genetic differentiation (i.e., F_{ST} or its linearized equivalent $F_{ST}/(1-F_{ST})$) at
274 the nuclear genome significantly increased with geographic distance in *An. gambiae* and *An. coluzzii*
275 (Lehmann, et al. 2003; The Ag1000G Consortium 2020). This isolation-by-distance (IBD) pattern was
276 significantly stronger in *An. coluzzii* than in *An. gambiae*, translating into reduced local effective
277 population size and/or reduced intergenerational dispersal distance in the first compared to the second
278 species (see Fig. 3 in The Ag1000G Consortium 2020). In line with these findings at the nuclear genome,

279 we found significant IBD at the mtDNA as well when considering all populations irrespective of the
280 species (Mantel's r = 0.35; p < 0.003; n=13), with a very strong signal among populations of *An. coluzzii*
281 (Mantel's r = 0.96; p = 0.017; n=5), and a weaker marginal signal among populations of *An. gambiae*
282 (Mantel's r = 0.32; p = 0.095; n=8) (Table S4). However, these analyses included populations that were
283 found genetically isolated by geographic barrier to geneflow when analyzing the nuclear genome (Angola
284 – AOM in *An. coluzzii*; Gabon - GAS and Mayotte Island - FRS in *An. gambiae*) (The Ag1000G Consortium
285 2020). These geographic barriers to dispersal can artificially inflate the IBD patterns without necessarily
286 implying reduced neighborhood size, which is the product of reduced local effective population density
287 and intergenerational dispersal distance that increase local genetic drift (Wright 1946; Rousset 1997). The
288 IBD signal among populations within species becomes weaker and not statistically different from zero
289 when removing geographically isolated populations (AOM, GAS, or FRS) from the IBD analysis (*An. coluzzii*
290 Mantel's r=0.46, p=0.167, n=4; *An. gambiae* Mantle's r=-0.18; p=0.617; n=6). Nevertheless, despite the
291 lack of significant results likely due to the small number of sampled populations, the strength of
292 association between genetic and geographic distances still remain strong and positive in *An. coluzzii* with
293 a r^2 value of 0.21, which is very comparable to the r^2 value of 0.22 observed at the nuclear genome (see
294 Fig. 3B in The Ag1000G Consortium 2020). This contrasts with the lack of any detectable IBD signal at the
295 mtDNA genome among populations of *An. gambiae* and the very weak IBD signal found on the nuclear
296 genome. These results are consistent with the distinct life history and dispersal strategies between the
297 two species (Dao, et al. 2014; Huestis, et al. 2019; Hemming-Schroeder, et al. 2020; Faiman, et al. 2022).
298 A significant fraction of the populations of *An. coluzzii* from NW Africa seem to endure locally the dry
299 season by engaging into aestivation strategy to rebound from local founders when the wet season starts.
300 In contrast, *An. gambiae* populations go locally extinct during the dry season and rebound after a certain
301 lag time by long-distance migration. Since female mosquitoes potentially disperse more and live also
302 longer than males (Yaro, et al. 2022), we may have expected weaker evidence of IBD at the mtDNA
303 compared to the signal found at the nuclear genome. However, we did not observe this effect. Thus, if
304 this effect exists, it would likely be counter balanced by the strong differences in aestivation and dispersal
305 strategies between the two species.
306
307 MtDNA variation in line with population demography of *An. gambiae* and *An. coluzzii*, but with an
308 imprint of the cryptic lineage history

309 Patterns of mtDNA variation among populations of *An. gambiae* and *An. coluzzii* (Table 1, Fig. 3) were
310 consistent with those previously reported at the nuclear genome (The Ag1000G Consortium 2020). The
311 exceptional genetic diversity previously observed at the nuclear genome also manifested at the mtDNA
312 level by a high overall level of haplotype diversity (*HD*=0.999), with 910 distinct haplotypes found in 1142
313 samples, an average number (K) of 58 differences between pairs of haplotypes, and 3017 segregating
314 sites including one third of singletons (Table 1).
315 Rarefaction curves, which account for differences in population sample sizes, for the number of
316 segregating sites (*S*) and the number of haplotypes (*H*) kept increasing with the sample size in most
317 populations. These curves clearly showed that the plateau was not within reach with a sampling up to 50,
318 especially for the populations located North of the Congo River Basin and West to the Rift Valley (Fig. 3).
319 In term of nucleotide diversity (π), these populations were also among the most diversified, with the
320 highest values observed for the *An. coluzzii* populations from the NW Africa, followed by the *An. gambiae*
321 populations from the same regions, and the hybrid (taxonomically uncertain) population in the Guinea
322 Bissau (GWA). These high levels of nucleotide diversity (π) actually reflected populations in which there
323 was a mixed proportion of haplotype from the cryptic and common mito-groups identified in the
324 phylogenetic analyses (Fig. 2). Nucleotide diversity (π) decreased in populations where the haplotype
325 mixture between cryptic and common lineages decreases, for example in the hybrid (taxonomically
326 uncertain) population of Gambia (GMS) where the cryptic lineage dominates or in the *An. gambiae*
327 population of Uganda (UGS) where it is almost absent. Overall, the high level of mtDNA variation
328 combined with very negative values for Tajima's D or Achaz's Y statistic (Achaz 2008) indicate an excess of
329 rare variants. These results support previous demographic inference modelling, showing large effective
330 population sizes in the NW Africa distribution ranges of the two species and evidence for historical
331 population expansions (The Ag1000G Consortium 2017, 2020). These conditions where genetic drift is
332 very ineffective are highly favorable to maintain high genetic diversity.
333 The (semi-)isolated populations from Gabon (*An. gambiae* – GAS) and Angola (*An. coluzzii* – AOM)
334 displayed intermediate values of genetic diversity and Tajima's D and Achaz's Y values closer to zero
335 (Table 1, Fig. 3). This is consistent with a historically more stable population size, and reduced effective
336 size as previously reported (The Ag1000G Consortium 2017, 2020). The two *An. gambiae* populations
337 from the islands of Mayotte (FRS) and Bioko (GQS) also departed from the other populations at the
338 mtDNA variation with very low nucleotide and haplotype diversity, and slightly negative Tajima's D and
339 Achaz's Y values. These are further evidence for small effective population size, and suggestive of strong
340 bottlenecks (or founder effects). In these island populations, the number of haplotypes was small and

341 closely related to each other, with excess of rare variants, as expected after strong bottlenecks which can
342 result from cyclic variation in population sizes, with possibly repeated founder events.
343 The taxonomically uncertain population from Kenyan (KEA) was already known for its very peculiar
344 patterns of genetic diversity at the nuclear genome, with specificities close to a colony population with
345 mixed ancestry from *An. gambiae* and *An. coluzzii* (see Fig. 4 in The Ag1000G Consortium 2020). The
346 Kenyan population was also an outlier population at the mtDNA genome with only four distinct
347 haplotypes detected that differ from each other at only ~32 sites with almost no singletons, thus a very
348 low haplotype diversity (HD=0.65) compared to the other populations, and the only population in the
349 Ag1000G sampling with highly positive Tajima's *D* and Achaz's *Y* values (Table 1, Fig. 3).
350

351 The cryptic mtDNA lineage: a phylogeographic legacy of the split between *An. gambiae* and *An.*
352 *coluzzii*

353 We investigated further the specificities of the distinctive cryptic mtDNA lineage (Fig. 2) to better
354 understand its potential evolutionary origin(s). We tested whether its occurrence was associated with the
355 potential occurrence of *Wolbachia* infection, the population genetic structure at the nuclear genome, as
356 estimated using a principal component analyses (PCA) following The Ag1000G Consortium (2017, 2020),
357 and other genomic features previously characterized for these samples, including major chromosomal
358 inversions ($2L^{a}$, $2R^{b,c,d,u}$), and insecticide resistance mutations (*rdl226*, *vgsc995*).

359 The intracellular and intraovarian *Wolbachia* bacterium is frequently found in insects and can be a
360 strong manipulator of insect reproductive biology, impacting physiology, behavior, creating cytoplasmic
361 incompatibilities, and could even act as a speciation agent (Rokas 2000; Werren, et al. 2008; Galtier, et al.
362 2009; Bruzzese, et al. 2021; Dong, et al. 2021; Dowling and Wolff 2023). *Wolbachia* can thus have
363 significant impacts on mitochondrial heritability and its genetic variation. It was previously detected in *An.*
364 *gambiae* and *An. coluzzii*, even though the vertical transmission or impacts on the reproductive biology of
365 these mosquitoes is still debated (Baldini, et al. 2014; Shaw, et al. 2016; Gomes, et al. 2017; Gomes and
366 Barillas-Mury 2018; Jeffries, et al. 2018; Pascar and Chandler 2018; Ayala, et al. 2019; Chrostek, et al.
367 2019; Straub, et al. 2020; Bamou, et al. 2021; Jeffries, et al. 2021).

368 We used the method of Pascar and Chandler (2018) to detect *Wolbachia* occurrence, using the
369 unmapped Illumina short-read data of the The Ag1000G Consortium (2020). Using a lenient set of filters
370 (at least 3 reads mapping to *Wolbachia* sequence with at least 90bp and 90% sequence identity), we

371 found 111 (9.7%) individual mosquitoes carrying reads blasting to the *Wolbachia* supergroup A (Fig. S9
372 and Table S5). This detection rate dropped to 27 (2.4%) positive individuals when using stricter detection
373 filters (3 reads blasting to Wolbachia sequences with at least 98bp length and 95% identity) similar to
374 those used by Pascar and Chandler (2018). *Wolbachia* was primarily detected in the *An. gambiae*
375 population of Mayotte (FRS; lenient: 83% or strict: 17%), and in the *An. coluzzii* populations of Côte
376 d'Ivoire (CIM; lenient: 55% or strict: 23%) and Ghana (GHM; lenient: 44% or strict: 4%) (Fig. S9 and Table
377 S5). These infection rates were quite low, especially if we consider the stricter criteria of Pascar and
378 Chandler (2018). These rates were in line with previous reports by Chrostek, et al. (2019) who even
379 questioned the natural occurrence of *Wolbachia* in natural populations of *An. gambiae* and *An. coluzzii.*
380 Chrostek, et al. (2019) argued that such a low number of reads could come from ingested food, or
381 mosquito parasites infected by *Wolbachia* (e.g. nematodes). We did not find any significant association
382 between the *Wolbachia* potential occurrence and the cryptic mtDNA lineage (ranked predictive power of
383 cross-features *x2y* metric = 0; Fig. S10).

384 Population genetic structure was estimated by a PCA on 100k independent single nucleotide
385 polymorphisms (SNPs) from the nuclear genome (Fig. S11), following the same procedure as in The
386 Ag1000G Consortium (2017, 2020). The PC1, PC6 and (to a lesser extent) PC2 were significant predictors
387 of the cryptic mtDNA lineage occurrence, explaining between 13% and 15% of the cryptic mtDNA lineage
388 variation for PC1, 21% for PC6, and 2% for PC2 (Fig. S10). PC1 discriminates *An. coluzzii* from *An. gambiae*,
389 PC6 splits the hybrid (taxonomically uncertain) populations from the other populations of *An. coluzzii* and
390 *An. gambiae*, and PC2 reflects the strong differentiation of the Angolan (AOM) population from the other
391 *An. coluzzii* and *An. gambiae* populations (Fig. S11). Altogether, these associations between the PCs and
392 the cryptic mtDNA lineage occurrence underline its variation according to species and geography visually
393 displayed in Fig. 4. Beside the PCs, no other genomic features tested here significantly correlated with the
394 occurrence of the cryptic mtDNA lineage variation in natural populations, except for the 2La
395 chromosomal inversion frequency. However, the 2La inversion was also strongly associated with the
396 population genetic structure capture by the PCs, suggesting its association with the cryptic mtDNA
397 lineage could be an "echo" of the population genetic structure (Fig. S10).

398 Taken together, all the above results suggest that the cryptic mtDNA lineage is likely a
399 phylogeographic legacy of the split between *An. colluzzii* and *An. gambiae*. It likely arose during a period
400 of isolation in *An. coluzzii,* as suggested by its level of divergence similar to the interspecific mtDNA
401 divergence observed between species of the AGC, and by the enrichment of this lineage in the

402 populations of *An. coluzzii* and in the taxonomically uncertain populations from the African *far-west* (Fig.
403 2). Together with the West to East gradient decline, these results suggest that the two sister species went
404 back into contact with an incomplete homogenization of the mtDNA gene pool.

405

406 Mito-nuclear interactions suggest selection on the mito-group divergence related to metabolic
407 resistance to pathogens and insecticides

408 Selection may have been involved in preventing a full homogenization of the mtDNA gene pool(s)
409 between *An. coluzzii, An. gambiae*, and the hybrid (taxonomically uncertain) populations, with possible
410 mito-nuclear interactions. To test this hypothesis, we conducted a genome-wide association study
411 (GWAS), testing which SNPs on the nuclear genome were significantly associated with the cryptic mtDNA
412 lineage occurrence (which is considered here as a binary variable). The GWAS was conducted considering
413 covariates including the 6 first PCs (Fig. S11) to account for population genetic structure, *Wolbachia*
414 occurrence (Table S5 and Fig. S9), and sex. As such analysis requires unrelated samples (Uffelmann, et al.
415 2021), we excluded closely related sample pairs in the Ag1000G dataset with kinship coefficient
416 exceeding the level of 2nd degree relatives (Table S6). The KING-robust method (Manichaikul, et al. 2010),
417 which relaxes the assumption of genetic homogeneity within population, identified multiple related pairs
418 of samples within populations equal or exceeding the level of 2nd degree relatives, with some cases of full-
419 sib or parent-offspring's, and even rare cases of monozygotic twins between pairs of mosquitoes (see Fig.
420 S12, S13, Table S7, and S8). Full-siblings or parent-offspring's relationships in mosquitoes can occur if
421 samples originated from larvae from a single female for example. Monozygotic twin's relationship can
422 either reflect sample duplicates in the dataset or highly inbred samples as would be observed in samples
423 coming from a laboratory colony. Unsurprisingly, the most impacted population was the Kenyan (KEA)
424 one. Its peculiar genetic make-up is similar to a laboratory colony, as was previously spotted in The
425 Ag1000G Consortium (2017). However, instances of full siblings and monozygotic twins were found in the
426 populations from Cameroon (CMS) and Angola (AOM) (see Fig. S12, S13, Table S7, and S8). Overall,
427 removing 98 samples from the dataset (Table S9) resolved all the issues allowing only up to the 3rd degree
428 relative association between sample pairs. The cleaned SNPs dataset used in the GWAS included 1044
429 unrelated samples (Fig. S11b) and 7,858,575 nuclear biallelic SNPs (Table S10). After removing related
430 samples, and accounting for population structure, sex, and *Wolbachia* occurrence as covariates, the
431 quantile-to-quantile plot and the genomic inflation factor (Lambda) was close to 1, indicating that the
432 genomic control of the GWAS was adequate (Fig. S14).

433 The GWAS identified 14 SNPs significantly associated with the cryptic mtDNA lineage occurrence
434 with *p-values* lower than the Bonferroni adjusted threshold of 4.4 10^{-8} (Fig. 4, S15, Table S11). Out of the
435 14 SNPs, seven were found close (within 1kb) or within transcripts, and two among them felt within two
436 annotated genes: *SCRASP1 (AGAP005625)* and *CYP6Z1 (AGAP008219).* The gene encoding for the
437 scavenger receptor *SCRASP1* was previously identified in *An. gambiae* as a prominent component
438 involved in immunity response to *Plasmodium* infection, but also other pathogens like bacteria (Danielli,
439 et al. 2000; Christophides, et al. 2002; Stathopoulos, et al. 2014; Smith, et al. 2016). By silencing this
440 gene, Smith, et al. (2016) showed it was an important modulator of *Plasmodium* development in *An.*
441 *gambiae*. These authors observed that *SCRASP1* was highly enriched after blood-feeding alone and
442 speculated that it may contribute to a metabolic pre-emptive immune response activated by the
443 hormonal changes that accompany blood feeding. Its role as cell surface receptors suggest it may act as
444 immuno-suppressors that when silenced, increase innate immune signaling in mosquito hemocyte
445 populations.

446 The second genes significantly associated with the cryptic mtDNA haplogroup occurrence was
447 *CYP6Z1*, encoding for a cytochrome P450 capable of metabolizing insecticide like the DDT in *An. gambiae*
448 (Chiu, et al. 2008). *CYP6Z1* is considered more generally as important insecticide resistance gene (Liu
449 2015; Ibrahim, et al. 2016).

450 We also identified two additional suggestive mito-nuclear association signals of interest on the X
451 chromosome, with a marginal *p-value* ranging between 5.3 10^{-8} and 1.4 10^{-7} (Fig. 4 and S16). The first one
452 (AGAP000561) is located at *ca.* 9.95Mb and encodes for a Piwi-interacting RNA (piRNA) previously
453 identified as part of "reproductive and development" cluster involved in germline development and
454 maintenance, spermatid development, oogenesis, and embryogenesis of *An. gambiae* (George, et al.
455 2015). The authors suggested these piRNA plays a significant role in the epigenetic regulation of the
456 reproductive processes in *An. gambiae*. AGAP000561 is an ortholog of the *D. melanogaster* kinesin heavy
457 chain (FBgn0001308), which plays a role in *oskar* mRNA localization to the pole plasm (Brendza, et al.
458 2000).

459 The second mito-nuclear marginal association signal of interest on the X chromosome was a clear
460 "skyscraper" located between 15.24Mb and 15.78Mb (Fig. 4). Zooming into this region revealed that the
461 signal contained two skyscrapers with the highest association signals that are nested within a broader
462 region with a distinctive elevation of the *p*-values (see Fig. S16). This distinctive region is not only of
463 special interests for being marginally associated with the cryptic mito-group split, but it was also

464 identified in many populations of *An. gambiae* and *An. coluzzii* with strong signal of recent positive
465 selection and association with metabolic insecticide resistance involving also the mitochondrial oxidative
466 phosphorylation (OXPHOS) respiratory chain (The Ag1000G Consortium 2017; Ingham, Tennessen, et al.
467 2021; Lucas, et al. 2023) (see also the *Ag1000G Selection Atlas, in prep;*
468 *https://malariagen.github.io/agam-selection-atlas/0.1-alpha3/index.html).* A total of 32 genes overlap
469 with this focal region (Fig. S16). Among them is the well-known cytochrome p450 encoded by *CYP9K1*, an
470 important metabolic insecticide resistance gene (Main, et al. 2015; Vontas, et al. 2018; Lucas, et al. 2023).
471 Even if that gene is within the elevated *p-value* region, it is located 62kb upstream from the first
472 skyscraper signal. The first highest signal overlapped with AGAP000820 (CPR125 - cuticular protein RR-2
473 family 125), AGAP00822 and AGAP00823 (CD81 antigen). The second skyscraper was centered close to
474 AGAP000840 (amiloride-sensitive sodium channel) and to AGAP000842 (NADH dehydrogenase
475 (ubiquinone). Other noteworthy genes in that genomic region included include AGAP000849 (NADH
476 dehydrogenase (ubiquinone) 1 beta subcomplex 1), and AGAP0008511 (cytochrome c oxidase subunit 6a,
477 mitochondria). These results thus suggest that the mtDNA lineage haplogroups are associated with
478 mitochondrial genes located in the nuclear genome, as well as genes involved directly or indirectly in
479 insecticide resistances mechanisms (cytochrome p450 and also cuticular regulation genes) and immunity.

480 Overall, these results support the hypothesis of a tight co-evolutionary history between the two
481 genomic compartments and suggest these mito-nuclear interactions left imprints on the mtDNA genetic
482 variation. The associations between the mtDNA lineages with genes involved in metabolic resistance to
483 pathogens (*Plasmodium* and bacteria) and insecticides support the emerging picture of the key role
484 played by mitochondria, and especially the OXSPHOS pathway in mosquito immunity and insecticide
485 resistance. Previous studies demonstrated that mitochondrial reactive oxygen species (mtROS) produced
486 by the OXSPHOS pathway modulate *An. gambiae* immunity against bacteria and *Plasmodium* (Molina-
487 Cruz, et al. 2008). Ingham, Brown, et al. (2021) were already discussing the disruption of parasite
488 development due to changes in redox state shown experimentally through reducing catalase activity
489 which in turn reduces oocyst density in the midgut (Molina-Cruz, et al. 2008), whilst the initial immune
490 response to parasite invasion consists in a strong mtROS burst (Molina-Cruz, et al. 2008; Castillo, et al.
491 2017).

492 Evidence implicating the mitochondrial respiration, OXPHOS pathway, and more generally the
493 mosquito metabolism into metabolic insecticide resistance is increasingly reported in the literature (e.g.,
494 Oliver and Brooke 2016; Ingham, Brown, et al. 2021; Ingham, Tennessen, et al. 2021; Lucas, et al. 2023).

495 Ingham, Tennessen, et al. (2021) used a multi-omics study to investigate the causative factors involved in
496 the re-establishment of pyrethroid resistance in a population of *An. coluzzii* colony from Burkina Faso
497 after a sudden loss of the insecticide resistance. Beside the involvement of the 2Rb inversion and of the
498 microbiome composition, the authors detected an increase in the genes expression within the OXPHOS
499 pathway in both resistant populations compared to the susceptible control, which translated
500 phenotypically into an increased respiratory rate and a reduced body size for resistant mosquitoes. This,
501 and previous studies (Oliver and Brooke 2016; Ingham, et al. 2017; Ingham, Brown, et al. 2021), clearly
502 indicated that elevated metabolism was linked directly with pyrethroid insecticide resistance.
503 Additionally, Lucas, et al. (2023) investigated novel loci associated with pyrethroid and organophosphate
504 resistance in *An. gambiae* and *An. coluzzii* using a GWAS, which also implicated the involvement of a wide
505 range of cytochrome p450, mitochondrial, and immunity genes (including also the same genomic region
506 on the X chromosome as the one we detected here). Both Ingham, Tennessen, et al. (2021) and Lucas, et
507 al. (2023) further pointed out possible cross-resistance mechanisms in metabolic insecticide resistance at
508 large, in which the mosquito metabolism, mitochondrial respiration, the OXPHOS pathway, and mtROS
509 production all seem to play a central role.

510

511 # Conclusions

512 In this study we showed that the determinants of mitochondrial genetic variation are multifarious and
513 complex. In agreement with previous studies (Fontaine, et al. 2015; Thawornwattana, et al. 2018; Müller,
514 et al. 2021), the mtDNA phylogeny clearly illustrated the previously reported highly reticulated
515 evolutionary history of the AGC. On one side, the three most widely distributed species – *An. gambiae*,
516 *An. coluzzii*, and *An. arabiensis* – form a rather homogeneous mtDNA gene pool clearly illustrating the
517 extensive level of introgression that occurred between them over the evolutionary timescale of the AGC.
518 On the other side, other species of the AGC cluster in a well diverged monophyletic clade, where each
519 species forms a clearly distinct monophyletic group. One haplotype in the mtDNA gene pool of *An.*
520 *gambiae* / *An. coluzzii* clustered close to *An. quadriannulatus,* in a position of the species tree where *An.*
521 *arabiensis* was placed according to the species informative loci on the X chromosome and the autosomes
522 (Fontaine, et al. 2015). This suggest that *An. arabiensis* mito-lineage might still be segregating in this
523 joined mtDNA gene pool of the three most widespread species in the AGC.

524 Mitochondrial introgression was also detected in other species, notably between *An. bwambae* and most
525 likely *An. gambiae*. The mitochondrial phylogenetic clustering of all the salt-water tolerant members of
526 the AGC (*An. merus, An. melas*, and *An. bwambae)* into a strongly supported monophyletic group also
527 departed from the admitted species branching order (Fontaine, et al. 2015; Thawornwattana, et al. 2018;
528 Barrón, et al. 2019). This suggests that historical mtDNA capture or selection from ancestral standing
529 genetic variation may have occurred, possibly involving selective processes related to specialization to a
530 very distinct salty larval habitat compared to the other fresh-water tolerant species of the AGC, and to
531 the majority of the *Anophelinae* species (Bradley 1994; Bradley 2008). A proper population genetic study
532 investigating this specialization from an evolutionary perspective still remains to be done.

533 Population structure, demography, and dispersal were found to be key drivers shaping the mtDNA
534 variation across the African populations of *An. gambiae* and *An. coluzzii*. The patterns identified mostly
535 followed those previously reported at the nuclear genomes (The Ag1000G Consortium 2017, 2020).
536 Despite the extensive level of gene flow between *An. gambiae* and *An. coluzzii*, significant variance
537 partitioning between species was still detectable. Even more striking was a clearly distinct mito-lineage
538 composed of 244 samples from *An. gambiae* and *An. coluzzii*. This lineage displayed a level of divergence
539 comparable to, yet slightly lower than, the mtDNA divergence observed between the species of the AGC.
540 Its distribution closely matched the distribution of *An. coluzzii* with a West-to-East and North-to-South
541 decreasing frequency gradient. This cryptic lineage appears to be a phylogeographic legacy of the species
542 isolation followed by a secondary contact between *An. gambiae* and *An. coluzzii* with incomplete
543 homogenization. Its frequency was clearly associated with species divergence (being enriched in *An.*
544 *coluzzii* compared to *An. gambiae*), mitochondrial level of diversity, and with population structure, but it
545 was not linked with the rare *Wolbachia* occurrence detected from the short-read data. Once accounting
546 for these variables in a GWAS-like study, we found significant associations between the cryptic lineage
547 occurrence and SNPs of the nuclear genome mostly from genes involved in metabolic resistance to
548 pathogens and insecticides. These results suggest that the phylogeographic split of mitochondrial lineages
549 and its incomplete re-homogenization after the secondary contact involved selective processes and a
550 certain mito-nuclear coevolution process between the two genome compartments. These associations
551 support the picture emerging in the recent literature underlining the key role played by the respiratory
552 metabolism, the OXPHOS pathway, and the generation of reactive oxygens in the metabolic resistance to
553 pathogens and to insecticides.

554 Cross-resistance mechanisms are increasingly recognized as a major threat to vector control strategy
555 allowing mosquitoes to adapt to insecticides (Ingham, Tennessen, et al. 2021; Lucas, et al. 2023). Our
556 results call for additional studies characterizing further the extent of mito-nuclear associations, the role of
557 mitochondria in adaptive processes to pathogens and insecticides, and a better understanding of the
558 tight coordination and co-evolution between the mitochondrial and nuclear genome. By integrating both
559 mtDNA and nuclear data, this study underlines that the mtDNA locus, once considered as a nearly neutral
560 locus and thus informative on the phylogenetic history of species, has in fact a much more complex
561 evolution in *Anopheles* mosquitoes where all the evolutionary forces (drift, migration, mutation and
562 multiple type of selection) interact. Such integration of nuclear and mito-genomic study are still rare, but
563 necessary to further our understanding of insect genomic evolution (Cameron 2014).

564

565 Materials and methods

566 Sampling and whole genome short read data

567 We retrieved whole genome short read (WG-SR) data (100 bp paired-end Illumina sequencing) from
568 74 mosquito specimens for six species of the AGC from Fontaine, et al. (2015), including *An. gambiae s.s,*
569 *An. coluzzii, An. arabiensis, An. quadriannulatus, An. melas, and An. merus*. As mtDNA genomes of these
570 samples were previously assembled, we compared them with the ones produced using the new pipeline
571 developped in the present study. We extracted reads that did not map to the nuclear reference genome
572 and used them to assemble mitogenome. We included also WG-SR data from three specimens of a seventh
573 species – *An. bwambae* – that were generated as part of the Anopheles 16 Genomes Project (Fontaine, et
574 al. 2015; Neafsey, et al. 2015). See the complete sampling details in Figure S1 and Table S1. We also
575 retrieved WG-SR data from The Ag1000G Consortium (2020) phase 2-AR1 release consisting of 1142 wild-
576 caught mosquito specimens including *An. gambiae s.s.* (n=720), *An. coluzzii* (n=283) and hybrid (n=139)
577 from 16 geographical sites (Figure 1, Table S2).

578 Previously generated *An. gambiae* reference mitochondial genome (GenBank ID: L20934.1) (Beard, et
579 al. 1993) was used to guide the assembly of the *AutoMitoG* pipeline. The mitochondrial sequences of *An.*
580 *christyi* and *An. epiroticus* from Fontaine, et al. (2015) were also included as outgroups sequences for
581 phylogeographic and phlogenetic analyses.

582

583 Mitochondrial genomes assembly and alignment

584 Information about the software versions is provided in Table S3. From the WG-SR files mapped to
585 nuclear reference genomes (bam files) obtained from Fontaine, et al. (2015) and The Ag1000G Consortium
586 (2020), we extracted reads that did not mapped to the nuclear reference genome and converted them to
587 paired-reads fastq files using *Samtools* (Li, et al. 2009) and *Picard* Tools
588 (http://broadinstitute.github.io/picard/). We wrote the *AutoMitoG* [*Automatic Mitochondrial Genome*
589 *assembly*] pipeline to streamline the mitochondrial genome assembly process (available at
590 https://github.com/jorgeamaya/automatic_genome_assembly, Fig. S2). As a general overview, the pipeline
591 starts by randomly sampling paired reads from each file at a 5% rate. Then, the pipeline proceeds to
592 assemble the mitogenome using a modified version of MITObim (Hahn, et al. 2013) (see details below) and
593 evaluate the quality of the assembly. This is done by counting the number of ambiguities outside the *D-*
594 *loop* control region; a region prone to sequencing and assembly errors due to the AT-rich homopolymer
595 sequences. If ambiguities remain in the mtDNA assembly, the previous steps are repeated iteratively,
596 increasing the sampling rate by 5% until the assembled mitogenomes shows no ambiguities or until 100%
597 of the reads are used. If ambiguities persist after reaching a sampling rate of 100%, the assembly with the
598 least number of ambiguities is selected by default. Finally, assembled mitogenome sequences together
599 with previously assembled reference genome (Beard, et al. 1993), and outgroup mtDNA sequences were
600 aligned to each other with MUSCLE (Edgar 2004).
601 The *AutoMitoG* pipeline relies on a modified version of MITObim (Hahn, et al. 2013) to assemble the
602 mtDNA genomes. Subsampling of the paired-reads is performed to achieve two purposes: (1) minimize the
603 number of ambiguous base calls – these result from conflicting pairing of reads from mitochondrial origin
604 with reads possibly originating from nuclear mitochondrial DNA copies (NUMTs), reads with sequencing
605 errors, and reads that originated from possible contamination. Since the number of reads from
606 mitochondrial origin is orders of magnitude larger in the WG-SR data than the number of reads from other
607 sources, subsampling safely reduces offending reads; (2) to normalize the dataset coverage, which speeds
608 up MITObim calculations, as the proportion of mitochondrial reads can differ between samples and studies.
609 Indeed, MITObim performs best with sequencing depth between 100 and 120x for Illumina reads (Hahn,
610 et al. 2013).
611 MITObim performs a two-steps assembly process (see Fig. 2 in Hahn, et al. (2013)). First, it maps reads
612 to a reference genome, here the mtDNA genome of *An. gambiae* from Beard, et al. (1993), to generate a
613 "backbone"; second, it extends this "backbone" with overlapping reads in an iterative *de novo* assembly
614 procedure. Thanks to its hybrid assembly strategy, MITObim perform well even if the samples and the
615 reference genome are phylogenetically distant (Hahn, et al. 2013). We forced majority consensus for non-

616 fully resolved calls during the backbone assembly and during the backbone iterative extension, for which
617 we customized MITObim's code. The original version of MITObim does not force majority consensus and
618 was not used in this study. However, it is included as an option in the pipeline for the benefit of users who
619 may prefer less stringent assembly criteria. See Fig. S2 for further information on the pipeline usage and
620 the corresponding documentation in the GitHub page.

621 We compare the newly assembled mitogenomes with those previously generated in Fontaine, et al.
622 (2015) (n=74). For that purpose, we first aligned mitogenome sequences from the two studies, cropped
623 out the control region (sequence length=14,844bp) following Fontaine, et al. (2015) as it is prone to
624 sequencing and assembly errors. Then, for each pair of mtDNA assemblies (new vs previous) coming from
625 each of the 74 samples in Fontaine, et al. (2015), we counted the number of pairwise differences. We also
626 visually compared assemblies generated with the two pipelines by building a distance-based neighbor-
627 joining tree (HKY genetic distance model) (Fig. S4). These steps were conducted in Geneious Prime®
628 (2023.0.1, Build 2022-11-28 12:49).

629

630 ## Mitogenome genetic diversity and phylogenetic relationships

631 As an initial assessment of the mtDNA alignment characteristics, we calculated various estimators of
632 genetic diversity per species and per location including: the number INDEL sites, segregating sites (S),
633 average number of differences between pairs of sequences (K), number of haplotypes (H), haplotype
634 diversity (HD), nucleotide diversity (π), Theta-Waterson (Θ_W), the Tajima's D, and the Achaz's Y (Achaz
635 2008). These statistics were computed using the C-library *libdiversity* developed by G. Achaz
636 (https://bioinfo.mnhn.fr/abi/people/achaz/cgi-bin/neutralitytst.c).

637 We estimated the phylogenetic relationships among mtDNA haplotypes using the same methodology
638 as in Fontaine et. al. (2015). We constructed mtDNA maximum likelihood (ML) phylogenies using RAxML
639 (parameters -m GTRGAMMA -# 1000 -T 16 -f a -x 12345 -p 12345). Bootstrap nodes' supports were
640 calculated using the fast-bootstrap method of RAxML (T 16 -# 1000 -f b -m GTRGAMMA). The mitogenome
641 sequences from *An. christy* and *An. epiroticus* were used as outgroups to root the trees. Multiple ML
642 phylogenetic trees were built: one only considering the 74 sequences from the *An. gambiae* species
643 complex for comparative purpose with previously published ML tree in Fontaine, et al. (2015), including
644 also the 3 *An. bwambae* samples; and another tree considering all the mitogenome sequences including
645 the 77 mitogenome sequences combined with the 1142 sequences of *An. gambiae* and *An. coluzzii* samples
646 from The Ag1000G Consortium (2020). To ease visualization, clades were collapsed when possible if they
647 contained multiple closely related samples.

648 In order to provide an alternative visualization of the phylogenetic relationships given the large size of
649 the total alignment, we also visualized mtDNA genetic variation among the 1142 sequences of *An. gambiae*
650 and *An. coluzzii* samples from The Ag1000G Consortium (2020) into a reduced multidimensional space
651 using a non-metric multidimensional scaling (nMDS). For that purposed, we calculated a *p*-distance matrix
652 among sequences using MEGA v.7 (Kumar, et al. 2016) and performed the nMDS using the *ecodist* R-
653 package (Goslee and Urban 2007). The nMDS results were further processed using *scikit*-learn v.0.22.1
654 (Pedregosa, et al. 2011) to identify major clusters in the data set, using a hierarchical clustering algorithm.
655

656 MtDNA genetic structure in natural populations of *An. gambiae* and *An. coluzzii*

657 We first assessed how the mtDNA variation of 1142 sequences of *An. gambiae* and *An. coluzzii* samples
658 from The Ag1000G Consortium (2020) partitioned among different levels of structuration using an analysis
659 of molecular variance (AMOVA) (Excoffier, et al. 1992). We considered 3 hierarchical levels of stratification:
660 between species, among populations within species, and within populations. The AMOVA was conducted
661 with the TN93+gamma model of sequence evolution using the *poppr R-package* (Kamvar, et al. 2014) and
662 the AMOVA function derived from the APE v5.6-4 R-package (Paradis, et al. 2004; Paradis and Schliep 2019).
663 Significance test was conducted using 1000 permutations. The analysis was conducted considering only
664 populations from the Ag1000G that were taxonomically unambiguous (n=938, see Fig. 1), thus removing
665 the hybrid taxonomic uncertain populations from The Gambiae (GMS) and Guinea-Bissau (GWA), as well as
666 the taxonomically uncertain population from Kenya (KEA).
667 Then, we quantified the level of genetic differentiation among populations by calculating the pairwise F_{ST}
668 differences using Arlequin v3.5 (Excoffier and Lischer 2010). We compared F_{ST} values obtained for the
669 mitochondrial DNA (mtDNA) with those previously reported for the nuclear genome (nDNA) (The Ag1000G
670 Consortium 2020).
671 We characterized further the mtDNA variation, comparing genetic diversity estimators for each species
672 at each locality. Since sample sizes vary among locations and can influence diversity estimators, we
673 performed a rarefaction procedure to account for differences in sample sizes (Hurlbert 1971; Kalinowski
674 2004, 2005; Szpiech, et al. 2008; Colwell, et al. 2012). To do so, sequences from each location were
675 randomly sampled incrementally, starting with three sequences up to a maximum of 50 sequences or until
676 there were no more sequences available for the specific location. This random sub-sampling with
677 replacement of the sequences was repeated 5000 times for each sample size increment (from 3 to 50) to
678 estimate the mean and standard error of the statistic of interest. This rarefaction analysis was applied for
679 estimating the standardized number of segregating site (*S*), the number of haplotypes (*H*), the nucleotide

680 diversity (π), the Tajima's *D*, and the Achaz's *Y* using python scripts and the *c-library libDiversity*. Results for
681 each statistic were summarized as rarefaction curves.
682 Isolation-by-distance (IBD) was computed following Rousset (1997). We derived the unbounded level of
683 genetic differentiation $F_{ST}/(1-F_{ST})$ between pairs of populations and correlated the genetic distance with the
684 geographic distance, expressed as the great circle distance (in $\log_{10}$ unit) globally across species, and also
685 for each species separately. The strength and significance of the IBD was tested using a Mantel test
686 implemented in *ade4* R-package (Dray and Dufour 2007) with 1000 permutations of the geographic
687 distance matrix. Since we were interested only in testing IBD within well-defined species, we removed the
688 hybrid and taxonomically ambiguous populations (The Gambia – GM, Guinea Bissau – GW, and Kenya –
689 KEA) from this analysis. Likewise, we ran the analysis with and without the island *An. gambiae* population
690 of Mayotte (FRS), as this population departs from the species' continuum (The Ag1000G Consortium 2020).
691

692 Detection of *Wolbachia* infection in natural populations of the Ag1000G

693 MtDNA variation can be strongly impacted by cytoplasmic conflict with the endosymbiont Wolbachia
694 (Galtier, et al. 2009; Dong, et al. 2021), and this latter has been reported in the AGC (Baldini, et al. 2014;
695 Shaw, et al. 2016; Gomes, et al. 2017; Gomes and Barillas-Mury 2018; Jeffries, et al. 2018; Ayala, et al. 2019;
696 Chrostek, et al. 2019; Straub, et al. 2020; Jeffries, et al. 2021). Therefore, we used the unmapped WG-SR
697 data to diagnose the infection status of each mosquito specimens of *An. gambiae* and *An. coluzzii* from the
698 Ag1000G phase-II (The Ag1000G Consortium 2020). To that end, we screened the unmapped Ag1000G
699 WG-SR data to detect *Wolbachia* specific sequences using MagicBlatst v.1.1.5 (NCBI) (Boratyn, et al. 2019)
700 following the procedure described in Pascar and Chandler (2018). WG-SR reads that did not map to the
701 nuclear reference genome were compared to selected reference *wsp*, *ftsZ*, and *groE* operon sequences
702 isolated from *Wolbachia* samples that are representative of supergroups A to D. For our analysis, we used
703 the *Wolbachia* sequence database of Pascar and Chandler (2018), which includes 61 sequences of
704 *Wolbachia* type A to D. We added four new sequences assembled by the authors to their database. These
705 are *Wolbachia* sequences of type B also found in *An. gambiae* specimens (Pascar & Chandler 2018). Using
706 the same *(strict)* detection criterion as in Pascar and Chandler (2018), a minimum of three reads with at
707 least 98bp length and 95% identity had to match with the same *Wolbachia* sequences for the specimen to
708 be considered as infected. We also applied a more "*lenient*" criterion: a minimum of three reads with at
709 least 90bp length and 90% identity had to match with the same *Wolbachia* sequences for the specimen to
710 be considered infected.
711

712 Mitogenome lineages associations with genomic features and with SNPs of the nuclear genome

713 We explored the associations between the two main mitochondrial phylogenetic lineages and the
714 genetic variation on the nuclear genome using the genome-wide SNP data from The Ag1000G Consortium
715 (2020). We also considered the association of the mtDNA lineages with other covariates including
716 population structure, *Wolbachia* infection status, and major chromosomal inversions. For that purpose, we
717 used a genome wide-like association study (GWAS) (Ansari, et al. 2017; Fellay and Pedergnana 2019),
718 considering the two main mtDNA lineages discovered in the phylogenetic analyses and how they are
719 associated with each SNP in the nuclear genome. This design aimed to assessing the extent of functional
720 associations between mtDNA lineages and the nuclear genome, highlighting potential mito-nuclear co-
721 evolution history, considering covariates, such as populations structure and *Wolbachia* infection status.

722 Following standard practices in GWAS (Uffelmann, et al. 2021), we first ensured that the samples
723 included in the Ag1000G were not too closely related. Therefore, we estimated the within population
724 kinship coefficients using KING 2.2.4 (Manichaikul, et al. 2010). The KING-robust approach relies on
725 relationships inference using high density SNP data to model genetic distance between pairs of individuals
726 as a function of their allele frequencies and kinship coefficient (Manichaikul, et al. 2010). This contrast with
727 other methods such as the one implemented in PLINK (Purcell, et al. 2007) which estimates relatedness
728 using estimator of pairwise identity-by-descent. However, this method is very sensitive to population
729 demography in contrast to KING-robust approach.

730 Following The Ag1000G Consortium (2017, 2020), we only used the free-recombining biallelic SNPs
731 (n=1,139,052) from section 15M to 41M of chromosome 3L to estimate pairwise kinship coefficients. This
732 genomic portion avoids non-recombining centromeric regions and major polymorphic chromosomal
733 inversions on chromosome 2, and the sex chromosome. No down sampling, nor linkage disequilibrium (LD)
734 pruning, nor any other preprocessing was undertaken on the data, following KING's authors
735 recommendation (Manichaikul, et al. 2010). We iteratively removed individuals with the largest number of
736 relationships above 2nd degree relative as estimated by KING. At any step, when two individuals were found
737 to have the same number of relationships, we removed the first individual according to its identifier's alpha
738 numeric order.

739 In order to include population structure as a covariate in the GWAS analysis, we conducted a principal
740 component analyses (PCA) following the same procedure as described in The Ag1000G Consortium (2017,
741 2020). We selected randomly 100,000 biallelic SNPs from the free-recombining part of the genome of *An.*
742 *gambiae* and *An. coluzzii* on chromosome 3L (from position 15Mb to 41Mb). To remain consistent with The
743 Ag1000G Consortium (2017, 2020), we followed the same filtering procedure. We performed a LD-pruning

744 using the function *locate_unlinked* from Python's module *scikit-allel* version 1.2.1 (Miles and Harding 2016)
745 to ensure independence among SNPs. Specifically, we scanned the genome in windows of 500bp slid by
746 steps 200bp and excluded SNPs with an $r^2 \geq 0.1$. This process was repeated 5 times to ensure most SNPs in
747 LD were removed. A PCA was then performed as described in The Ag1000G Consortium (2017, 2020), using
748 *scikit-allel* version 1.2.1 (Miles and Harding 2016). Results were plotted highlighting specimens according
749 to their locality of origin. PC scores were stored and used as covariates in the GWAS analysis.

750 Prior to the actual GWAS analysis, we assessed the extent of association between the two identified
751 major mtDNA phylogenetic lineages, the specimens' sex, *Wolbachia* infection status, and population
752 structure as estimated by the top six PC axes from the PCA. We also considered the inversion karyotypes
753 as reported by The Ag1000G Consortium (2020) and (Love, et al. 2019). Given the diverse nature of
754 covariables, we calculated a proxy of the Pearson's correlation coefficient between variables capable of
755 handling numerical and categorical variable types using the *x2y*-metric (Ramakrishnan 2021; Lares
756 2023). The *x2y*-metric performs a linear regression on continuous response variables and a classification
757 procedure on categorical response variables. Then, it uses the calculated model to predict the data based
758 on the independent variable and, finally, estimates a percentage of error in the predictions. As this method
759 does not provide any significance test with a *p*-value, the 95% confidence interval was calculated using
760 1000 permutations.

761 Finally, we conducted the formal GWAS-like analysis to evaluate the associations between the two main
762 mtDNA phylogenetic lineages and the nuclear SNP genotype variation, considering the following covariates:
763 the population structure using PC-scores, the *Wolbachia* infection status, and sex. We performed the GWAS
764 using the program *SNPTEST* v2.5.4-beta3 (Marchini *et al.* 2007). The main mtDNA lineage were used as
765 "phenotype values" defined as the phylogenetic mtDNA clusters from the hierarchical clustering of the
766 NMDS analysis. After normalization, we used the PC scores of the PCA obtained from S*cikit-allele* as
767 continuous covariates, *Wolbachia* infection status and sex as binary covariates. Only unrelated samples
768 (n=1053) and SNPs with a MAF ≥ 0.01 (n=7,858,575, Table 10) were considered in this analysis. The
769 threshold to assess the significance of the GWAS was defined following a Bonferroni corrected *p*-value
770 accounting for the number of independent genomic blocks in the genome (0.05/1,139,052 = 4.39e-8). The
771 number of independent genomic blocks in our data set was approximated by the number of independent
772 SNPs as determined with Plink v 1.90 (Table S10). The results of the GWAS were plotted as Manhattan and
773 QQ-plots in R.

774 We produced a list of genes IDs that contained one or more significant SNPs from the GWAS within the
775 CDS or within 1kb upstream or downstream from the CDS according to the general feature format file

776 VectorBase-57_AgambiaePEST.gff from *VectorBase* release 57, 2022-APR-21 (Giraldo-Calderon, et al.
777 2015). The list of genes was then used to extract information associated to such genes from *VectorBase*.
778

779 ## Acknowledgment

780 We would like to acknowledge the *Anopheles gambiae* 1000 genomes consortium
781 (https://www.malariagen.net/projects/ag1000g#people), and especially Nick Harding, Mara K.N.
782 Lawniczak, Martine Donnelly, Dominic P. Kwiatkowski (deceased), Carlo Costantini, Nora J. Besansky, and
783 Frédéric Labbé for providing resources, supports, and help during the development of this study. We also
784 thank the Center for Information Technology of the University of Groningen for their support and for
785 providing access to the *Peregrine* high-performance computing cluster. We also wish to acknowledge the
786 ISO 9001 certified IRD *i-Trop* HPC (member of the South Green Platform) at IRD Montpellier for providing
787 HPC resources that have contributed to the research results reported within this paper
788 (https://bioinfo.ird.fr; www.southgreen.fr).

789

790 ## Author contribution

791 MCF designed research; JEAR and MCF performed research; AM, CC, YBC, VP contributed new
792 data/reagents/analytic tools; AM and CC curated the original data of the Ag1000G phase-2; JEAR, MCF,
793 YBC, CC analyzed data; MCF and BW provided supervision and funding; MCF wrote the paper; all the
794 authors provided inputs and feedbacks.

795

796 ## Data availability

797 Short-read data used in this study to assemble mitogenomes come from two consortium projects: the
798 MalariaGEN *Anopheles gambiae* 1000 genomes projects phase-2 AR1 data release
799 (https://www.malariagen.net/data/ag1000g-phase-2-ar1; see also The Ag1000G Consortium (2020)); and
800 the Anopheles 16 genomes project (Fontaine, et al. 2015; Neafsey, et al. 2015) (National Center for
801 Biotechnology Information, NIH, BioProject IDs: PRJNA67511 and PRJNA254046). Mitochondrial genome
802 sequences have been deposited on NCBI and the mitogenome alignment on the IRD DataSud repository:
803 https://doi.org/10.23708/XXXXX. The *AutoMitoG* pipeline, codes and scripts used in this study are
804 available via github (https://github.com/jorgeamaya/automatic_genome_assembly and
805 https://github.com/jorgeamaya/malaria_mitogenome).

806 **REFERENCES**
807

808 Achaz G. 2008. Testing for neutrality in samples with sequencing errors. Genetics 179:1409-1424.

809 Allio R, Donega S, Galtier N, Nabholz B. 2017. Large Variation in the Ratio of Mitochondrial to Nuclear
810 Mutation Rate across Animals: Implications for Genetic Diversity and the Use of Mitochondrial DNA as a
811 Molecular Marker. Mol Biol Evol 34:2762-2772.

812 Ansari MA, Pedergnana V, L C Ip C, Magri A, Von Delft A, Bonsall D, Chaturvedi N, Bartha I, Smith D,
813 Nicholson G, et al. 2017. Genome-to-genome analysis highlights the effect of the human innate and
814 adaptive immune systems on the hepatitis C virus. Nature Genetics 49:666-673.

815 Ayala D, Acevedo P, Pombi M, Dia I, Boccolini D, Costantini C, Simard F, Fontenille D. 2017. Chromosome
816 inversions and ecological plasticity in the main African malaria mosquitoes. Evolution 71:686-701.

817 Ayala D, Akone-Ella O, Rahola N, Kengne P, Ngangue MF, Mezeme F, Makanga BK, Nigg M, Costantini C,
818 Simard F, et al. 2019. Natural Wolbachia infections are common in the major malaria vectors in Central
819 Africa. Evol Appl 12:1583-1594.

820 Baldini F, Segata N, Pompon J, Marcenac P, Shaw WR, Dabire RK, Diabate A, Levashina EA, Catteruccia F.
821 2014. Evidence of natural Wolbachia infections in field populations of Anopheles gambiae. Nat Commun
822 5:3985.

823 Bamou R, Diarra AZ, Mayi MPA, Djiappi-Tchamen B, Antonio-Nkondjio C, Parola P. 2021. Wolbachia
824 Detection in Field-Collected Mosquitoes from Cameroon. Insects 12:1133.

825 Barrón MG, Paupy C, Rahola N, Akone-Ella O, Ngangue MF, Wilson-Bahun TA, Pombi M, Kengne P,
826 Costantini C, Simard F, et al. 2019. A new species in the major malaria vector complex sheds light on
827 reticulated species evolution. Scientific Reports 9.

828 Bazin E, Glemin S, Galtier N. 2006. Population size does not influence mitochondrial genetic diversity in
829 animals. Science 312:570-572.

830 Beard CB, Hamm DM, Collins FH. 1993. The mitochondrial genome of the mosquito Anopheles gambiae:
831 DNA sequence, genome organization, and comparisons with mitochondrial sequences of other insects.
832 Insect Molecular Biology 2:103-124.

833 Besansky NJ, Lehmann T, Fahey GT, Fontenille D, Braack LEO, Hawley WA, Collins FH. 1997. Patterns of
834 mitochondrial variation within and between African malaria vectors, Anopheles gambiae and An.
835 arabiensis, suggest extensive gene flow. Genetics 147.

836 Boratyn GM, Thierry-Mieg J, Thierry-Mieg D, Busby B, Madden TL. 2019. Magic-BLAST, an accurate RNA-
837 seq aligner for long and short reads. BMC Bioinformatics 20:405

838 Bradley TJ. 1994. The role of physiological capacity, morphology, and phylogeny in determining habitat
839 use in mosquitoes. In: Wainwright PC, Reilly SM, editors. Ecological Morphology. Chicago, IL: University
840 of Chicago Press. p. 303-318.

841 Bradley TJ. 2008. Saline-water insects: ecology, physiology and evolution. In: Lancaster J, Briers RA,
842 editors. Aquatic Insects. Oxford, UK: CAB International.

843 Brendza RP, Serbus LR, Duffy JB, Saxton WM. 2000. A function for kinesin I in the posterior transport of
844 oskar mRNA and Staufen protein. Science 289:2120-2122.

845 Bruzzese DJ, Schuler H, Wolfe TM, Glover MM, Mastroni JV, Doellman MM, Tait C, Yee WL, Rull J, Aluja
846 M, et al. 2021. Testing the potential contribution of Wolbachia to speciation when cytoplasmic
847 incompatibility becomes associated with host-related reproductive isolation. Molecular Ecology
848 31:2935-2950.

849 Caccone A, Garcia BA, Powell JR. 1996. Evolution of the mitochondrial DNA control region in the
850 Anopheles gambiae complex. Insect Molecular Biology 5:51-59.

851 Cameron SL. 2014. Insect mitochondrial genomics: implications for evolution and phylogeny. Annu Rev
852 Entomol 59:95-117.

853 Castillo JC, Ferreira ABB, Trisnadi N, Barillas-Mury C. 2017. Activation of mosquito complement
854 antiplasmodial response requires cellular immunity. Science Immunology 2:eaal1505.

855 Cheng C, Tan JC, Hahn MW, Besansky NJ. 2018. Systems genetic analysis of inversion polymorphisms in
856 the malaria mosquito Anopheles gambiae. Proc Natl Acad Sci U S A 115:E7005-E7014.

857 Cheng C, White BJ, Kamdem C, Mockaitis K, Costantini C, Hahn MW, Besansky NJ. 2012. Ecological
858 Genomics of Anopheles gambiae Along a Latitudinal Cline: A Population-Resequencing Approach.
859 Genetics 190:1417-1432.

860 Chiu T-L, Wen Z, Rupasinghe SG, Schuler MA. 2008. Comparative molecular modeling of Anopheles
861 gambiae CYP6Z1, a mosquito P450 capable of metabolizing DDT. Proceedings of the National Academy
862 of Sciences 105:8855-8860.

863 Christophides GK, Zdobnov E, Barillas-Mury C, Birney E, Blandin S, Blass C, Brey PT, Collins FH, Danielli A,
864 Dimopoulos G, et al. 2002. Immunity-related genes and gene families in Anopheles gambiae. Science
865 298:159-165.

866 Chrostek E, Gerth M, Moran NA. 2019. Is Anopheles gambiae a Natural Host of Wolbachia? mBio
867 10:e00784-00719.

868 Clarkson CS, Weetman D, Essandoh J, Yawson AE, Maslen G, Manske M, Field SG, Webster M, Antão T,
869 MacInnis B, et al. 2014. Adaptive introgression between Anopheles sibling species eliminates a major
870 genomic island but not reproductive isolation. Nature Communications 5:4248.

871 Coetzee M, Hunt RH, Wilkerson R, Della Torre A, Coulibaly MB, Besansky NJ. 2013. Anopheles coluzzii
872 and Anopheles amharicus, new members of the Anopheles gambiae complex. Zootaxa 3619:246-274.

873 Coluzzi M, Sabatini A, della Torre A, Di Deco MA, Petrarca V. 2002. A polytene chromosome analysis of
874 the *Anopheles gambiae* species complex. Science 298:1415-1418.

875 Colwell RK, Chao A, Gotelli NJ, Lin SY, Mao CX, Chazdon RL, Longino JT. 2012. Models and estimators
876 linking individual-based and sample-based rarefaction, extrapolation and comparison of assemblages.
877 Journal of Plant Ecology 5:3-21.

878 Costantini C, Ayala D, Guelbeogo WM, Pombi M, Some CY, Bassole IHN, Ose K, Fotsing J-M, Sagnon NF,
879 Fontenille D, et al. 2009. Living at the edge: biogeographic patterns of habitat segregation conform to
880 speciation by niche expansion in Anopheles gambiae. BMC Ecology 9:16.

881 Crawford JE, Riehle MM, Guelbeogo WM, Gneme A, Sagnon NF, Vernick KD, Nielsen R, Lazzaro BP. 2015.
882 Reticulate Speciation and Barriers to Introgression in theAnopheles gambiaeSpecies Complex. Genome
883 Biology and Evolution 7:3116-3131.

884 Danielli A, Loukeris TG, Lagueux M, Muller HM, Richman A, Kafatos FC. 2000. A modular chitin-binding
885 protease associated with hemocytes and hemolymph in the mosquito Anopheles gambiae. Proc Natl
886 Acad Sci U S A 97:7136-7141.

887 Dao A, Yaro AS, Diallo M, Timbine S, Huestis DL, Kassogue Y, Traore AI, Sanogo ZL, Samake D, Lehmann
888 T. 2014. Signatures of aestivation and migration in Sahelian malaria mosquito populations. Nature
889 516:387-390.

890 Ding YR, Yan ZT, Si FL, Li XD, Mao QM, Asghar S, Chen B. 2020. Mitochondrial genes associated with
891 pyrethroid resistance revealed by mitochondrial genome and transcriptome analyses in the malaria
892 vector Anopheles sinensis (Diptera: Culicidae). Pest Manag Sci 76:769-778.

893 Dong Z, Wang Y, Li C, Li L, Men X, Reddy GVP. 2021. Mitochondrial DNA as a Molecular Marker in Insect
894 Ecology: Current Status and Future Prospects. Annals of the Entomological Society of America 114:470-
895 476.

896 Donnelly MJ, Licht MC, Lehmann T. 2001. Evidence for recent population expansion in the evolutionary
897 history of the malaria vectors Anopheles arabiensis and Anopheles gambiae. Mol Biol Evol 18:1353-
898 1364.

899 Dowling DK, Wolff JN. 2023. Evolutionary genetics of the mitochondrial genome: insights from
900 Drosophila. Genetics 224:iyad036.

901 Dray S, Dufour A-B. 2007. The ade4 Package: Implementing the Duality Diagram for Ecologists. Journal of
902 Statistical Software 22:10.18637/jss.v18022.i18604.

903 Edgar RC. 2004. MUSCLE: multiple sequence alignment with high accuracy and high throughput. Nucleic
904 Acids Res 32:1792-1797.

905 Excoffier L, Lischer HE. 2010. Arlequin suite ver 3.5: a new series of programs to perform population
906 genetics analyses under Linux and Windows. Mol Ecol Resour 10:564-567.

907 Excoffier L, Smouse PE, Quattro JM. 1992. Analysis of molecular variance inferred from metric distances
908 among DNA haplotypes: application to human mitochondrial DNA restriction data. Genetics 131:479-
909 491.

910 Faiman R, Yaro AS, Dao A, Sanogo ZL, Diallo M, Samake D, Yossi O, Veru LM, Graber LC, Conte AR, et al.
911 2022. Isotopic evidence that aestivation allows malaria mosquitoes to persist through the dry season in
912 the Sahel. Nature Ecology & Evolution 6:1687-1699.

913 Fellay J, Pedergnana V. 2019. Exploring the interactions between the human and viral genomes. Human
914 Genetics 139:777-781.

915 Fontaine MC, Pease JB, Steele A, Waterhouse RM, Neafsey DE, Sharakhov IV, Jiang X, Hall AB,
916 Catteruccia F, Kakani E, et al. 2015. Mosquito genomics. Extensive introgression in a malaria vector
917 species complex revealed by phylogenomics. Science 347:1258524.

918 Galtier N, Nabholz B, Glemin S, Hurst GD. 2009. Mitochondrial DNA as a marker of molecular diversity: a
919 reappraisal. Mol Ecol 18:4541-4550.

920 George P, Jensen S, Pogorelcnik R, Lee J, Xing Y, Brasset E, Vaury C, Sharakhov IV. 2015. Increased
921 production of piRNAs from euchromatic clusters and genes in Anopheles gambiae compared with
922 Drosophila melanogaster. Epigenetics Chromatin 8:50.

923 Giraldo-Calderon GI, Emrich SJ, MacCallum RM, Maslen G, Dialynas E, Topalis P, Ho N, Gesing S,
924 VectorBase C, Madey G, et al. 2015. VectorBase: an updated bioinformatics resource for invertebrate
925 vectors and other organisms related with human diseases. Nucleic Acids Res 43:D707-713.

926 Gomes FM, Barillas-Mury C. 2018. Infection of anopheline mosquitoes with Wolbachia: Implications for
927 malaria control. PLoS Pathog 14:e1007333.

928 Gomes FM, Hixson BL, Tyner MDW, Ramirez JL, Canepa GE, Alves ESTL, Molina-Cruz A, Keita M, Kane F,
929 Traore B, et al. 2017. Effect of naturally occurring Wolbachia in Anopheles gambiae s.l. mosquitoes from
930 Mali on Plasmodium falciparum malaria transmission. Proc Natl Acad Sci U S A 114:12566-12571.

931 Goslee SC, Urban DL. 2007. The ecodist Package for dssimilarity-based analysis of ecological data.
932 Journal of Statistical Software 22:10.18637/jss.v18022.i18607.

933 Grau-Bové X, Lucas E, Pipini D, Rippon E, van ‘t Hof AE, Constant E, Dadzie S, Egyir-Yawson A, Essandoh J,
934 Chabi J, et al. 2021. Resistance to pirimiphos-methyl in West African Anopheles is spreading via
935 duplication and introgression of the Ace1 locus. PLOS Genetics 17:e1009253.

936 Grau-Bové X, Tomlinson S, O’Reilly AO, Harding NJ, Miles A, Kwiatkowski D, Donnelly MJ, Weetman D,
937 Rogers R. 2020. Evolution of the Insecticide Target Rdl in African Anopheles Is Driven by Interspecific and
938 Interkaryotypic Introgression. Molecular Biology and Evolution 37:2900-2917.

939 Hahn C, Bachmann L, Chevreux B. 2013. Reconstructing mitochondrial genomes directly from genomic
940 next-generation sequencing reads – a baiting and iterative mapping approach. Nucleic Acids Research
941 41:e129.

942 Hanemaaijer MJ, Houston PD, Collier TC, Norris LC, Fofana A, Lanzaro GC, Cornel AJ, Lee Y. 2018.
943 Mitochondrial genomes of Anopheles arabiensis, An. gambiae and An. coluzzii show no clear species
944 division. F1000Res 7:347.

945 Hemming-Schroeder E, Zhong D, Machani M, Nguyen H, Thong S, Kahindi S, Mbogo C, Atieli H, Githeko
946 A, Lehmann T, et al. 2020. Ecological drivers of genetic connectivity for African malaria vectors
947 Anopheles gambiae and An. arabiensis. Sci Rep 10:19946.

948 Huestis DL, Dao A, Diallo M, Sanogo ZL, Samake D, Yaro AS, Ousman Y, Linton YM, Krishna A, Veru L, et
949 al. 2019. Windborne long-distance migration of malaria mosquitoes in the Sahel. Nature 574:404-408.

950 Hurlbert SH. 1971. The Nonconcept of Species Diversity: A Critique and Alternative Parameters. Ecology
951 52:577-586.

952 Hurst GD, Jiggins FM. 2005. Problems with mitochondrial DNA as a marker in population,
953 phylogeographic and phylogenetic studies: the effects of inherited symbionts. Proc Biol Sci 272:1525-
954 1534.

955 Ibrahim SS, Ndula M, Riveron JM, Irving H, Wondji CS. 2016. The P450 CYP6Z1 confers
956 carbamate/pyrethroid cross-resistance in a major African malaria vector beside a novel carbamate-
957 insensitive N485I acetylcholinesterase-1 mutation. Mol Ecol 25:3436-3452.

958 Ingham VA, Brown F, Ranson H. 2021. Transcriptomic analysis reveals pronounced changes in gene
959 expression due to sub-lethal pyrethroid exposure and ageing in insecticide resistance Anopheles coluzzii.
960 BMC Genomics 22:337.

961 Ingham VA, Pignatelli P, Moore JD, Wagstaff S, Ranson H. 2017. The transcription factor Maf-S regulates
962 metabolic resistance to insecticides in the malaria vector Anopheles gambiae. BMC Genomics 18:669.

963 Ingham VA, Tennessen JA, Lucas ER, Elg S, Yates HC, Carson J, Guelbeogo WM, Sagnon NF, Hughes GL,
964 Heinz E, et al. 2021. Integration of whole genome sequencing and transcriptomics reveals a complex
965 picture of the reestablishment of insecticide resistance in the major malaria vector *Anopheles coluzzii*.
966 PLOS Genetics 17:e1009970.

967 Jeffries CL, Cansado-Utrilla C, Beavogui AH, Stica C, Lama EK, Kristan M, Irish SR, Walker T. 2021.
968 Evidence for natural hybridization and novel Wolbachia strain superinfections in the Anopheles gambiae
969 complex from Guinea. R Soc Open Sci 8:202032.

970 Jeffries CL, Lawrence GG, Golovko G, Kristan M, Orsborne J, Spence K, Hurn E, Bandibabone J, Tantely
971 LM, Raharimalala FN, et al. 2018. Novel Wolbachia strains in Anopheles malaria vectors from Sub-
972 Saharan Africa. Wellcome Open Research 3:113.

973 Kalinowski ST. 2004. Counting Alleles with Rarefaction: Private Alleles and Hierarchical Sampling
974 Designs. Conservation Genetics 5:539-543.

975 Kalinowski ST. 2005. hp-rare 1.0: a computer program for performing rarefaction on measures of allelic
976 richness. Molecular Ecology Notes 5:187-189.

977 Kamvar ZN, Tabima JF, Grunwald NJ. 2014. Poppr: an R package for genetic analysis of populations with
978 clonal, partially clonal, and/or sexual reproduction. PeerJ 2:e281.

979 Kumar S, Stecher G, Tamura K. 2016. MEGA7: Molecular Evolutionary Genetics Analysis Version 7.0 for
980 Bigger Datasets. Mol Biol Evol 33:1870-1874.

981 Lares B. 2023. lares: R Package for Analytics and Machine Learning
982 (https://laresbernardo.github.io/lares/) Last accessed: 2023/03/15. Version 5.2.1.9000.

983 Lee Y, Marsden CD, Norris LC, Collier TC, Main BJ, Fofana A, Cornel AJ, Lanzaro GC. 2013. Spatiotemporal
984 dynamics of gene flow and hybrid fitness between the M and S forms of the malaria mosquito,
985 Anopheles gambiae. Proc Natl Acad Sci U S A 110:19854-19859.

986 Lehmann T, Licht M, Elissa N, Maega BT, Chimumbwa JM, Watsenga FT, Wondji CS, Simard F, Hawley
987 WA. 2003. Population Structure of Anopheles gambiae in Africa. J Hered 94:133-147.

988 Li H, Handsaker B, Wysoker A, Fennell T, Ruan J, Homer N, Marth G, Abecasis G, Durbin R, Genome
989 Project Data Processing S. 2009. The Sequence Alignment/Map format and SAMtools. Bioinformatics
990 25:2078-2079.

991 Liu N. 2015. Insecticide Resistance in Mosquitoes: Impact, Mechanisms, and Research Directions. Annual
992 Review of Entomology 60:537-559.

993 Loughlin SO. 2020. The expanding Anopheles gambiae species complex. Pathog Glob Health 114:1.

994 Love RR, Redmond SN, Pombi M, Caputo B, Petrarca V, Della Torre A, Anopheles gambiae Genomes C,
995 Besansky NJ. 2019. In Silico Karyotyping of Chromosomally Polymorphic Malaria Mosquitoes in the
996 Anopheles gambiae Complex. G3: Genes, Genomes, Genetics 9:3249-3262.

997 Lucas ER, Nagi SC, Egyir-Yawson A, Essandoh J, Dadzie S, Chabi J, Djogbénou LS, Medjigbodo AA, Edi CV,
998 Ketoh GK, et al. 2023. Genome-wide association studies reveal novel loci associated with pyrethroid and
999 organophosphate resistance in *Anopheles gambiae s.l.* bioRxiv:10.1101/2023.1101.1113.523889.

1000 Main BJ, Lee Y, Collier TC, Norris LC, Brisco K, Fofana A, Cornel AJ, Lanzaro GC. 2015. Complex genome
1001 evolution in Anopheles coluzzii associated with increased insecticide usage in Mali. Mol Ecol 24:5145-
1002 5157.

1003 Manichaikul A, Mychaleckyj JC, Rich SS, Daly K, Sale M, Chen WM. 2010. Robust relationship inference in
1004 genome-wide association studies. Bioinformatics 26:2867-2873.

1005 Miles A, Harding NJ. 2016. *Scikit-allel*: a Python package for exploratory analysis of large scale genetic
1006 variation data. https://github.com/cggh/scikit-allel, last accessed 16/11/2022 Version 1.2.1: Zenodo.

1007 Molina-Cruz A, DeJong RJ, Charles B, Gupta L, Kumar S, Jaramillo-Gutierrez G, Barillas-Mury C. 2008.
1008 Reactive Oxygen Species Modulate Anopheles gambiae Immunity against Bacteria and Plasmodium.
1009 Journal of Biological Chemistry 283:3217-3223.

1010 Müller NF, Ogilvie HA, Zhang C, Fontaine MC, Amaya-Romero JE, Drummond AJ, Tanja S. 2021. Joint
1011 inference of species histories and gene flow. bioRxiv:10.1101/348391.

1012 Neafsey DE, Christophides GK, Collins FH, Emrich SJ, Fontaine MC, Gelbart W, Hahn MW, Howell PI,
1013 Kafatos FC, Lawson D, et al. 2013. The Evolution of the Anopheles 16 Genomes Project. G3
1014 Genes|Genomes|Genetics 3:1191-1194.

1015 Neafsey DE, Waterhouse RM, Abai MR, Aganezov SS, Alekseyev Ma, Allen JE, Amon J, Arca B,
1016 Arensburger P, Artemov G, et al. 2015. Highly evolvable malaria vectors: The genomes of 16 Anopheles
1017 mosquitoes. Science 347:1258522.

1018 Nguyen THM, Tinz-Burdick A, Lenhardt M, Geertz M, Ramirez F, Schwartz M, Toledano M, Bonney B,
1019 Gaebler B, Liu W, et al. 2023. Mapping mitonuclear epistasis using a novel recombinant yeast
1020 population. PLOS Genetics 19:e1010401.

1021 Nwakanma DC, Neafsey DE, Jawara M, Adiamoh M, Lund E, Rodrigues A, Loua KM, Konate L, Sy N, Dia I,
1022 et al. 2013. Breakdown in the process of incipient speciation in Anopheles gambiae. Genetics 193:1221-
1023 1231.

1024 Oliver SV, Brooke BD. 2016. The Role of Oxidative Stress in the Longevity and Insecticide Resistance
1025 Phenotype of the Major Malaria Vectors Anopheles arabiensis and Anopheles funestus. PLoS One
1026 11:e0151049.

1027 Paradis E, Claude J, Strimmer K. 2004. APE: Analyses of Phylogenetics and Evolution in R language.
1028 Bioinformatics 20:289-290.

1029 Paradis E, Schliep K. 2019. ape 5.0: an environment for modern phylogenetics and evolutionary analyses
1030 in R. Bioinformatics 35:526-528.

1031 Pascar J, Chandler CH. 2018. A bioinformatics approach to identifying Wolbachia infections in
1032 arthropods. PeerJ 6:e5486.

1033 Pedregosa F, Varoquaux G, Gramfort A, Michel V, Thirion B, Grisel O, Blondel M, Prettenhofer P, Weiss
1034 R, Dubourg V, et al. 2011. Scikit-learn: Machine Learning in Python. Journal of Machine Learning
1035 Research 12:2825-2830.

1036 Pombi M, Kengne P, Gimonneau G, Tene-Fossog B, Ayala D, Kamdem C, Santolamazza F, Guelbeogo
1037 WM, Sagnon NF, Petrarca V, et al. 2017. Dissecting functional components of reproductive isolation
1038 among closely related sympatric species of the Anopheles gambiae complex. Evolutionary Applications
1039 10:1102-1120.

1040 Purcell S, Neale B, Todd-Brown K, Thomas L, Ferreira MA, Bender D, Maller J, Sklar P, de Bakker PI, Daly
1041 MJ, et al. 2007. PLINK: a tool set for whole-genome association and population-based linkage analyses.
1042 Am J Hum Genet 81:559-575.

1043 Ramakrishnan R. 2021. An Alternative to the Correlation Coefficient That Works For Numeric and
1044 Categorical Variables (https://rviews.rstudio.com/2021/04/15/an-alternative-to-the-correlation-
1045 coefficient-that-works-for-numeric-and-categorical-variables/), Last accesseed 2023/03/15.

1046 Rand DM, Mossman JA, Zhu L, Biancani LM, Ge JY. 2018. Mitonuclear epistasis, genotype-by-
1047 environment interactions, and personalized genomics of complex traits in Drosophila. IUBMB Life
1048 70:1275-1288.

1049 Riehle MM, Bukhari T, Gneme A, Guelbeogo WM, Coulibaly B, Fofana A, Pain A, Bischoff E, Renaud F,
1050 Beavogui AH, et al. 2017. The Anopheles gambiae 2La chromosome inversion is associated with
1051 susceptibility to Plasmodium falciparum in Africa. eLife 6:e25813.

1052 Rokas A. 2000. Wolbachia as a speciation agent. Trends in Ecology & Evolution 15:44-45.

1053 Rousset F. 1997. Genetic differentiation and estimation of gene flow from F-statistics under isolation by
1054 distance. Genetics 145:1219-1228.

1055 Sayre RG. 2013. A new map of standardized terrestrial ecosystems of Africa. Washington, DC: American
1056 Association of Geographers.

1057 Shaw WR, Marcenac P, Childs LM, Buckee CO, Baldini F, Sawadogo SP, Dabire RK, Diabate A, Catteruccia
1058 F. 2016. Wolbachia infections in natural Anopheles populations affect egg laying and negatively
1059 correlate with Plasmodium development. Nat Commun 7:11772.

1060 Simard F, Ayala D, Kamdem GC, Pombi M, Etouna J, Ose K, Fotsing JM, Fontenille D, Besansky NJ,
1061 Costantini C. 2009. Ecological niche partitioning between Anopheles gambiae molecular forms in
1062 Cameroon: The ecological side of speciation. BMC Ecology 9:17.

1063 Sloan DB, Fields PD, Havird JC. 2015. Mitonuclear linkage disequilibrium in human populations.
1064 Proceedings of the Royal Society B: Biological Sciences 282:20151704.

1065 Smith RC, King JG, Tao D, Zeleznik OA, Brando C, Thallinger GG, Dinglasan RR. 2016. Molecular Profiling
1066 of Phagocytic Immune Cells in Anopheles gambiae Reveals Integral Roles for Hemocytes in Mosquito
1067 Innate Immunity. Mol Cell Proteomics 15:3373-3387.

1068 Stathopoulos S, Neafsey DE, Lawniczak MK, Muskavitch MA, Christophides GK. 2014. Genetic dissection
1069 of Anopheles gambiae gut epithelial responses to Serratia marcescens. PLoS Pathog 10:e1003897.

1070 Straub TJ, Shaw WR, Marcenac P, Sawadogo SP, Dabire RK, Diabate A, Catteruccia F, Neafsey DE. 2020.
1071 The Anopheles coluzzii microbiome and its interaction with the intracellular parasite Wolbachia. Sci Rep
1072 10:13847.

1073 Szpiech ZA, Jakobsson M, Rosenberg NA. 2008. ADZE: a rarefaction approach for counting alleles private
1074 to combinations of populations. Bioinformatics 24:2498-2504.

1075 Tennessen JA, Ingham VA, Toe KH, Guelbeogo WM, Sagnon N, Kuzma R, Ranson H, Neafsey DE. 2021. A
1076 population genomic unveiling of a new cryptic mosquito taxon within the malaria-transmitting
1077 Anopheles gambiae complex. Mol Ecol 30:775-790.

1078 Thawornwattana Y, Dalquen D, Yang Z. 2018. Coalescent Analysis of Phylogenomic Data Confidently
1079 Resolves the Species Relationships in the Anopheles gambiae Species Complex. Mol Biol Evol 35:2512-
1080 2527.

1081 The Ag1000G Consortium. 2017. Genetic diversity of the African malaria vector Anopheles gambiae.
1082 Nature 552:96-100.

1083 The Ag1000G Consortium. 2020. Genome variation and population structure among 1142 mosquitoes of
1084 the African malaria vector species Anopheles gambiae and Anopheles coluzzii. Genome Research
1085 30:1533–1546.

1086 The Ag1000G Consortium. 2021. MalariaGEN Anopheles gambiae1000 genomes phase 3 data release.
1087 MalariaGEN:https://www.malariagen.net/data/ag1000g-phase1003-snp.

1088 Thelwell NJ, Huisman RA, Harbach RE, Butlin RK. 2000. Evidence for mitochondrial introgression
1089 between Anopheles bwambae and Anopheles gambiae. Insect Molecular Biology 9:203-210.

1090 Uffelmann E, Huang QQ, Munung NS, de Vries J, Okada Y, Martin AR, Martin HC, Lappalainen T,
1091 Posthuma D. 2021. Genome-wide association studies. Nature Reviews Methods Primers 1:59.

1092 Van Leeuwen T, Vanholme B, Van Pottelberge S, Van Nieuwenhuyse P, Nauen R, Tirry L, Denholm I.
1093 2008. Mitochondrial heteroplasmy and the evolution of insecticide resistance: non-Mendelian
1094 inheritance in action. Proc Natl Acad Sci U S A 105:5980-5985.

1095 Vicente JL, Clarkson CS, Caputo B, Gomes B, Pombi M, Sousa CA, Antao T, Dinis J, Botta G, Mancini E, et
1096 al. 2017. Massive introgression drives species radiation at the range limit of Anopheles gambiae. Sci Rep
1097 7:46451.

1098 Vontas J, Grigoraki L, Morgan J, Tsakireli D, Fuseini G, Segura L, Niemczura de Carvalho J, Nguema R,
1099 Weetman D, Slotman MA, et al. 2018. Rapid selection of a pyrethroid metabolic enzyme CYP9K1 by
1100 operational malaria control activities. Proceedings of the National Academy of Sciences 115:4619-4624.

1101 Werren JH, Baldo L, Clark ME. 2008. Wolbachia: master manipulators of invertebrate biology. Nat Rev
1102 Microbiol 6:741-751.

1103 White BJ, Collins FH, Besansky NJ. 2011. Evolution of Anopheles gambiae in Relation to Humans and
1104 Malaria. Annual Review of Ecology, Evolution, and Systematics 42:111-132.

1105 Wolff JN, Ladoukakis ED, Enriquez JA, Dowling DK. 2014. Mitonuclear interactions: evolutionary
1106 consequences over multiple biological scales. Philos Trans R Soc Lond B Biol Sci 369:20130443.

1107 World Health Organization. 2022. World malaria report 2022. In. Geneva. p. 293.

1108 Wright S. 1946. Isolation by distance under diverse systems of mating. Genetics 31:39-59.

1109 Yaro AS, Linton Y-M, Dao A, Diallo M, Sanogo ZL, Samake D, Ousmane Y, Kouam C, Krajacich BJ, Faiman
1110 R, et al. 2022. Diversity, composition, altitude, and seasonality of high-altitude windborne migrating
1111 mosquitoes in the Sahel: Implications for disease transmission. Frontiers in Epidemiology 2:1001782.
1112

1113

Main text tables and Figures

Table captions

Table 1. Mitochondrial genetic diversity statistics per species and population for the entire mitogenome alignment (14,844 bps). Number of sequences (N), INDEL sites (INDELS), segregating sites (S), singletons (*Sing.*), shared polymorphism (*Shared P.*), average number of differences between pairs of sequences (K), number of haplotypes (H), haplotype diversity (HD), nucleotide diversity (π), Theta-Waterson (Θ_W), Tajima's D, number (and proportion) of sequences belonging to the cryptic lineage (N (%) Cryptic).

Table 2. Analysis of Molecular Variance (AMOVA) describing the variance partitioning at three hierarchical levels: between species, between populations within species, and within populations. The AMOVA was conducted with the TN93+gamma model of sequence evolution. The analysis was conducted considering only populations from the Ag1000G that were taxonomically unambiguous (n=938, see Fig. 1), thus removing the uncertain populations from The Gambiae (GMS) and Guinea-Bissau (GWA), as well as the population from Kenya (KEA). The table provide the main results of the AMOVA including the degree of freedom (Df) at each level, the sum square and mean square deviations (SSD and MSD), variance component (σ), and variance proportion (%), ϕ-statistics, and *p*-value from 1000 permutation test.

1133 Table 1. Mitochondrial genetic diversity statistics per species and population for the entire mitogenome alignment (14,844 bps). Number
1134 of sequences (N), INDEL sites (INDELS), segregating sites (S), singletons (*Sing.*), shared polymorphism (*Shared P.*), average number of
1135 differences between pairs of sequences (K), number of haplotypes (H), haplotype diversity (HD), nucleotide diversity (π), Theta-
1136 Waterson (Θ_W), Tajima's D, number (and proportion) of sequences belonging to the cryptic lineage (N (%) Cryptic).

Species	**Group**	**Location**	***N***	***INDELS***	***S***	***Sing.***	***Shared P.***	***K***	***H***	***HD***	***π***	Θ_W	***Tajima's D****	***N (%) Cryptic***
All	*All*	All	1142	14	3017	1195	1822	57.5	910	0.999	0.0039	0.0266	-2.50*	232 (20%)
Hybrid	*Hybrid*	*Hybrid*	156	2	942	468	474	53.8	131	0.997	0.0036	0.0113	-2.23*	77 (49%)
An.coluzzii	*An.coluzzii*	*An.coluzzii*	283	4	1298	541	757	60	237	0.998	0.0040	0.014	-2.24*	89 (31%)
An.gambiae	*An.gambiae*	*An.gambiae*	655	10	2336	1004	1332	54.3	539	0.999	0.0037	0.0222	-2.51*	66 (10%)
An.coluzzii	AOM	Angola	78	2	323	121	202	37.5	50	0.983	0.0025	0.0044	-1.48	4 (5%)
An.coluzzii	BFM	Burkina Faso	75	1	819	489	330	59.7	75	1.000	0.0040	0.0113	-2.25*	37 (49%)
An.coluzzii	CIM	Côte d'Ivoire	71	0	552	260	292	58.6	58	0.988	0.0040	0.0077	-1.71*	27 (38%)
An.coluzzii	GHM	Ghana	55	1	498	224	274	61.6	53	0.998	0.0041	0.0073	-1.57*	20 (36%)
An.coluzzii	GNM	Guinea	4	0	61	61	0	30.5	2	0.500	0.0021	0.0022	-0.87*	1 (25%)
An.gambiae	BFS	Burkina Faso	92	2	1019	585	434	56.9	91	1.000	0.0038	0.0135	-2.46*	10 (11%)
An.gambiae	CMS	Cameroon	297	8	1537	639	898	56.6	217	0.996	0.0038	0.0164	-2.41*	47 (16%)
An.gambiae	FRS	Mayotte	24	0	31	18	13	5.3	15	0.920	0.0004	0.0006	-1.35	0 (0%)
An.gambiae	GAS	Gabon	69	0	283	117	166	38.3	48	0.972	0.0026	0.004	-1.23	2 (3%)
An.gambiae	GHS	Ghana	12	0	215	149	66	48.4	11	0.985	0.0033	0.0048	-1.5	1 (8%)
An.gambiae	GNS	Guinea	40	2	574	357	217	57.3	38	0.997	0.0039	0.0091	-2.16*	4 (10%)
An.gambiae	GQS	Bioko Island	9	0	78	48	30	22.8	9	1.000	0.0015	0.0019	-1.06	0 (0%)
An.gambiae	UGS	Uganda	112	3	949	519	430	49.8	112	1.000	0.0034	0.0121	-2.44*	2 (2%)
Hybrid	GMS	The Gambia	65	0	364	140	224	47.8	43	0.982	0.0032	0.0052	-1.33	42 (65%)
Hybrid	GWA	Guinea Bissau	91	2	792	436	356	55.7	88	0.999	0.0038	0.0105	-2.20*	35 (38%)
Uncertain	KEA	Kenya	48	0	81	1	80	32.3	4	0.650	0.0022	0.0012	2.74	0 (0%)

1137 * Star on Tajima's D values indicates a significant departure from neutrality (D≠0) based on 1000 coalescent simulations.

Table 2. Analysis of Molecular Variance (AMOVA) describing the variance partitioning at three hierarchical levels: between species, between populations within species, and within populations. The AMOVA was conducted with the TN93+gamma model of sequence evolution. The analysis was conducted considering only populations from the Ag1000G that were taxonomically unambiguous (n=938, see Fig. 1), thus removing the hybrid taxonomically uncertain populations from The Gambiae (GMS) and Guinea-Bissau (GWA), as well as the population from Kenya (KEA). The table provide the main results of the AMOVA including the degree of freedom (Df) at each level, the sum square and mean square deviations (SSD and MSD), variance component (σ), and variance proportion (%), ϕ-statistics, and *p*-value from 1000 permutation test.

	Df	SSD	MSD	Var (Sigma)	Variation (%)	ϕ	P-value
ϕ_{CT} (between species)	1	0.0492	0.0492	6.96E-05	3.4	0.03	<0.007
ϕ_{SC} (among populations within species)	11	0.1535	0.0140	1.94E-04	9.6	0.10	<0.001
ϕ_{ST} (within populations)	925	1.6267	0.0018	1.76E-03	87.0	0.13	<0.001
Total	937	1.8294	0.0020	2.02E-03	100	-	-

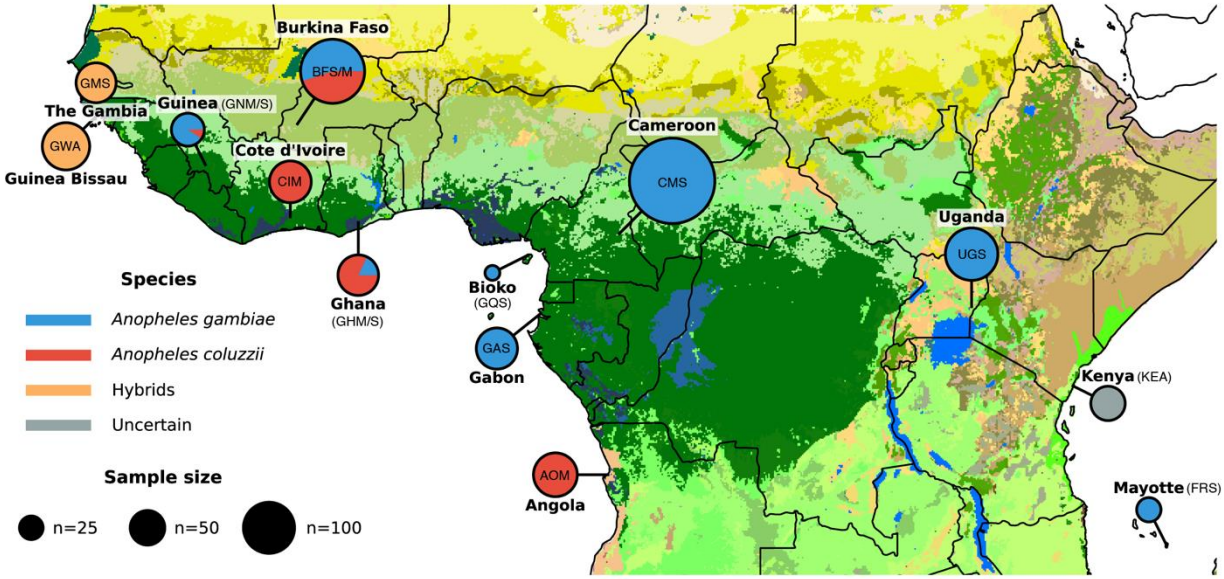

Figure 1. Approximate sampling locations and sample size per location of the 1142 samples of *An. gambiae* and *An. coluzzii* from the The Ag1000G Consortium (2020).

The population codes are also provided within or next to the pie-charts (see Table 1 and S2). Colors within the pie-charts describe the species and include: An. *gambiae* (in blue; formerly the *S-form* of *An. gambiae*), *An. coluzzii* (in red; formerly known as the M-form of *An. gambiae*), the hybrid taxonomically uncertain populations of the African *far-west* (in orange), and the taxonomically uncertain population of Kenya (in grey). The figure is modified from The Ag1000G Consortium (2020). Map colors represent ecosystem classes; dark green designates forest ecosystems. For a compete color legend see Figure 9 in the work of Sayre (2013). (see Table S2 for further details on the sampling).

Figure 2. Phylogenetic relationships among mitogenomes.
(A) MtDNA maximum likelihood phylogeny based on the 1222 sequences composed of the 1142 *An. gambiae and An. coluzzii* samples from the Ag1000G, 77 from the 7 species of the AGC from Fontaine et al (2015), on reference sequence from *An. gambiae*, and the two outgroups. (Black dots: An. *gambiae (An. gam), An. coluzzii (An. col), or An. arabiensis (An. ara), Green: An. merus (An. mer), Blue: An. melas (An. mel), Purple, An. quadriannulatus (An. qua), Pink: An. bwambae).* Bootstrap support values (%) are indicated at the nodes. Notice the absence of *An. arabiensis* specific mtDNA haplotype, the monophyletic clustering of the salt-water tolerent species (SWAT in green), the introgressed bwambae3 sample within within *An. gambiae* and *An. coluzzii* clade (in pink), and the presence of one *An. gambiae* individual (AN0293 CMS, orange arrow) next to *An. quadriannulatus,* in a place where *An. arabiensis* would be expected based on the admitted species tree (Fontaine et al. 2015). **(B)** Distance-based nMDS analysis of the 1142 mtDNA sequences from the Ag1000G with a color-coding based on a hierarchical clustering analysis. The cryptic lineage is in yellow. The outlier sample at the bottom is AN0293_C CMS is most likely a relic of *An. arabiensis* haplotype (see Fig. 2A). None of the samples associated with bwambae3 (AB0015 from BFM, AG0145 from GMS, and AY0038 CIM) were found in the cryptic lineage. **(C)** Geographic distribution of the cryptic lineage.

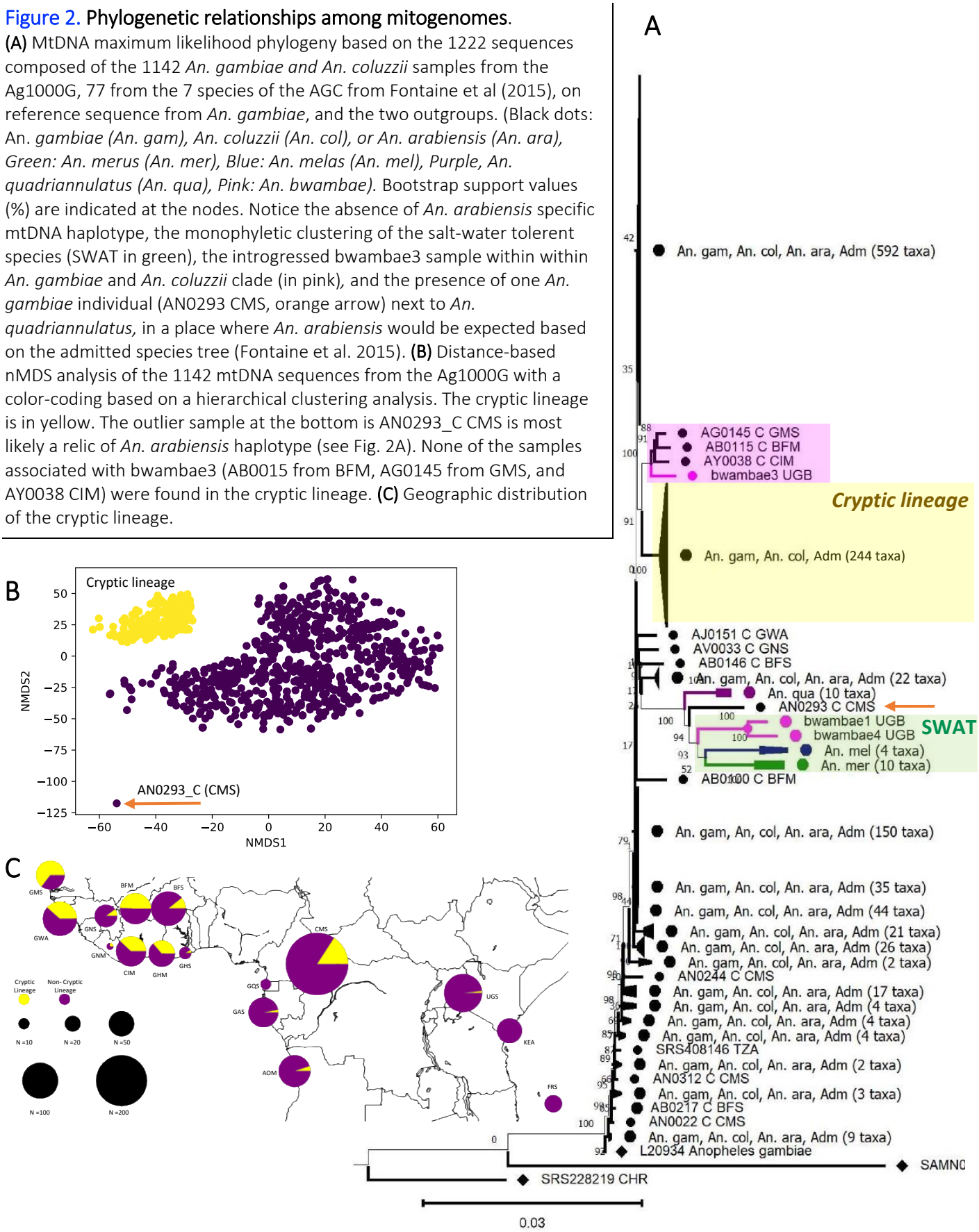

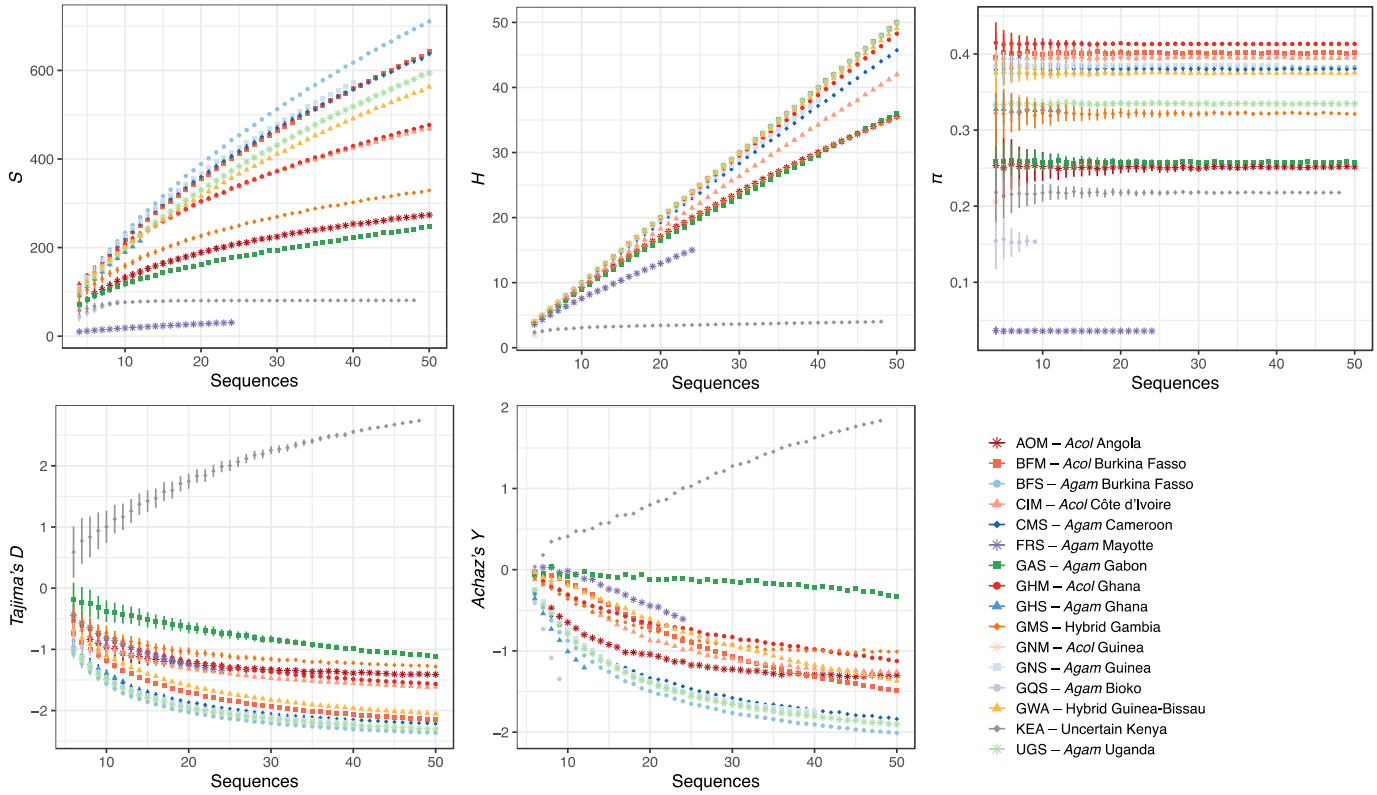

Figure 3. **Mitochondrial genetic diversity statistics for each population of the Ag1000G.** The statistics shown include the number of segregating site (*S*), the number of haplotypes (*H*), the nucleotide diversity (π), the Tajima's *D*, and the Achaz's *Y*. The rarefaction curves describe the impact of varying sample size on the estimated values for each statistic and for each population. The mean and standard error values are reported for each sample size increment from 3 to 50.

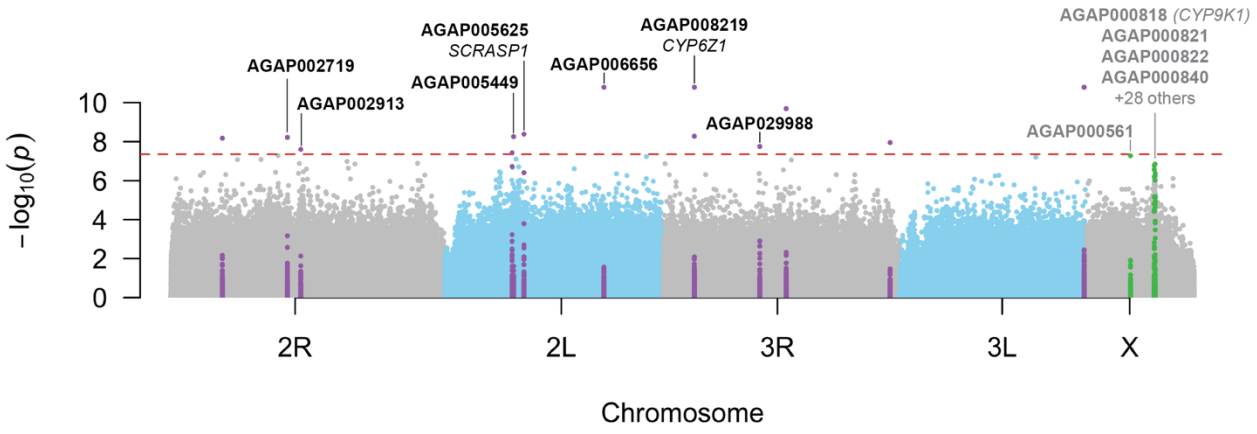

Figure 4. Manhattan plot showing the genetic associations between the two major mtDNA lineages and each of the SNPs on the nuclear genome.

The GWAS was conducted accounting for population structure using the 6 first PCs, sex, and *Wolbachia* occurrence as covariates. Each chromosome arms are colored-coded. The red dash horizontal line shows the Bonferroni corrected significance threshold of 4.4 10^{-8}. The 14 significant SNPs together with the SNPs 1kb upstream or downstream are marked in purple. SNPs in green are those marginally significant on the X chromosome forming a clear "skyscraper". Gene-ID and gene name, when an annotated transcript was available, are displayed. See fig. S14 for QQ-plot, fig. S15 for a zoomed view of each significant SNPs, and fig. S16 for a zoomed view on the X-chromosome.